PERFORMANCE AND LOADS CORRELATION OF A UH-60A SLOWED ROTOR AT HIGH ADVANCE RATIOS

Sesi Kottapalli
Flight Vehicle Research and Technology Division
NASA Ames Research Center
Moffett Field, California
sesi.kottapalli@nasa.gov

Measured data from the slowed-rotor 2010 UH-60A Airloads Rotor test in the NASA Ames 40- by 80- Foot Wind Tunnel are compared with CAMRAD II calculations. The emphasis is to correlate overall trends. This analytical effort considers advance ratios from 0.3 to 1.0, with the rotor rotational speed at 40%NR. The rotor performance parameters considered are the thrust coefficient, power coefficient, L/D_E, torque, and H-force. The blade loads considered are the half peak-to-peak, mid-span and outboard torsion, flatwise, and chordwise moments, and the pitch link load. For advance ratios ≤ 0.7, the overall trends for the performance and loads (excluding the pitch link load) could be captured, but with substantial overprediction or underprediction. The correlation gradually deteriorates as the advance ratio is increased and for advance ratios ≥ 0.8 there is no correlation. The pitch link load correlation is not good. There is considerable scope for improvement in the prediction of the blade loads. Considering the modeling complexity associated with the unconventional operating condition under consideration, the current predictive ability to capture overall trends is encouraging.

Notation

C_H	Rotor H-force coefficient
C_L	Rotor lift coefficient
C_P	Rotor power coefficient
C_Q	Rotor torque coefficient
C_T	Rotor thrust coefficient
H-force	Rotor drag in shaft axes, lb
L/D_E	Rotor lift to effective drag ratio
NP	Integer (N) multiple of rotor speed
R	Rotor radius, ft
V	Forward speed, ft/sec
%NR	% of normal rotor rotational speed
α_s	Rotor shaft angle, deg
μ	Rotor advance ratio ($V/\Omega R$)
σ	Rotor solidity ratio
Ω	Rotor rotational speed, rad/sec

Introduction

In 2010, NASA and the U.S. Army completed a full-scale wind tunnel test of the heavily instrumented UH-60A Airloads Rotor, Ref. 1. During this test, in addition to normal advance ratio flight conditions, high advance ratio conditions were also explored and experimental data acquired at advance ratios up to $\mu = 1.0$. To increase the advance ratio, the UH-60A rotor RPM was slowed down to as low as 40%NR (data were also acquired at 65%NR). In the current study, the measured high advance ratio performance and rotor loads data at 40%NR are compared with analytical predictions. This effort is currently a work in progress. In 2008, the experimental and theoretical performances of three different rotors, excluding the UH-60A, were studied using five analyses, Ref. 2. Recently, the 2010 UH-60A test data were carefully studied to obtain a fundamental understanding of the various physical phenomena associated with the high advance ratio operating condition, Ref. 3.

The emphasis in this initial study is on correlating *overall trends*. Since the slowed rotor condition is an unconventional operating condition, the paper includes both dimensional and non-dimensional comparisons of the measurements and predictions. An eventual goal is to identify the limits of comprehensive analyses, and assess whether the current aerodynamic representations of large regions of reverse flow, etc. are sufficiently appropriate or if computational fluid dynamics, CFD, is needed. Overall, the paper includes rotor performance correlations of the type shown in Ref. 2. This enables an assessment of the correlation level currently achievable for the UH-60A using comprehensive analyses relative to the Ref. 2 correlation level.

The present study considers the first step in the prediction of the reduced RPM UH-60A performance and rotor loads. A fixed, rigid hub is considered, i.e. the effects of the wind tunnel test stand, the Large Rotor Test Apparatus, LRTA, are not included. The rotorcraft comprehensive analysis CAMRAD II, Refs. 4-6, is used to produce analytical predictions. The most recent UH-60A CAMRAD II rotor model is used in this study, Ref. 7.

Measured Wind Tunnel Data

Reference 1 contains a description of the UH-60A slowed

Presented at the American Helicopter Society Future Vertical Lift Aircraft Design Conference, January 18-20, 2012, San Francisco, California.

rotor testing conducted in the National Full-Scale Aerodynamics Complex (NFAC) 40- by 80-Foot Wind Tunnel.

Analytical Model

The CAMRAD II model used is briefly described as follows. The model includes an elastic blade. The UH-60A rotor blade is modeled using elastic beam elements, with each element having two elastic flap bending, two elastic lag bending, and two torsion degrees of freedom. The blade consists of four beam elements. For the rotor trim procedure, 12 blade modes are used. The analytical trim procedure is similar to the wind tunnel test trim procedure for high advance ratio slowed rotors, i.e., given an advance ratio and collective pitch, the lateral and longitudinal cyclics are adjusted to minimize the blade 1P flapping. At higher advance ratios it became necessary to relax the flapping tolerance in order to get converged results. The prescribed (rigid) wake model is used. At present, the UH-60A control system stiffness is based on the flight test article, Ref. 7. Any differences associated with the current wind tunnel configuration have not been accounted for in this study.

Results

Correlations of the performance and loads for $\mu = 0.3$ to 1.0 at a rotor rotational speed 40%NR (approximately 104 RPM) and shaft angle $\alpha_s = 0^o$ are shown in this paper.

Figure 1 shows the calculated frequency fan plot for the UH-60A rotor. At 40%NR, the first elastic chordwise mode ("Chord 2" in the figure) and the torsion mode are close to each other, in the range 10P -12P, Table 1.

In the correlation figures that follow, the predictions are shown in solid blue lines and the measurements are shown in solid red lines. Also, for each correlation parameter, the vertical axis scale is kept the same at all advance ratios for easier comparison.

Rotor performance

Figures 2-6 show the performance correlations for $\mu = 0.3$ to 1.0, listed as follows:

a) Thrust coefficient C_T/σ versus collective, Figs. 2a-h.
b) Power coefficient C_P/σ versus C_T/σ, Figs. 3a-h
c) Rotor lift to effective drag L/D_E versus C_L/σ, Figs. 4a-h
d) Torque versus C_T/σ, Figs. 5a-h
e) H-force versus C_T/σ, Figs. 6a-h.

For the thrust coefficient C_T/σ, Figs. 2a-g show that both test and analysis have roughly the same linear trend with collective. However, the analysis underpredicts C_T/σ, and at high μ ($\mu = 0.7$, Fig. 2e), this results in an equivalent discrepancy (delta) of 2^o in the collective pitch. It appears that the slope of C_T/σ with respect to the collective decreases as the advance ratio is increased. Also, at $\mu = 1.0$, Fig. 2h, the thrust coefficient C_T/σ has a very small value, approximately 0.02 and is independent of the collective.

Figures 3a-e show that the analysis captures the measured power coefficient C_P/σ nonlinear trend with C_T/σ for $\mu \leq 0.7$, with substantial overprediction at high μ. For $\mu \geq 0.8$, there is no correlation, Figs. 3f-h.

Figures 4a-e show that the analysis captures the measured rotor L/D_E trends for $\mu \leq 0.7$, with substantial overprediction at high μ. For $\mu \geq 0.8$, there is no correlation, Figs. 4f-h. For the C_T/σ range under consideration, approximately 0.01 to 0.11, the L/D_E ratio goes from ≤ 2 to ≥ 8, Figs. 4a-h. The effective drag D_E depends on the accurate determination of both the profile and induced drag contributions, thus complicating the prediction of L/D_E. This merits further study since the accurate prediction of L/D_E is extremely important in the estimation of aircraft range.

Figures 5a-c show that the dimensional rotor torque is well predicted at low μ for this low rotor speed, 104 RPM, condition. As expected, the torque and the power coefficient, Figs. 5a-e and 3a-e, have similar trends, i.e., nonlinear increase with C_T/σ, and similar to the power coefficient correlation, the analysis captures the measured rotor torque trends for $\mu \leq 0.7$, Figs. 5a-e, with substantial overprediction at high μ. For $\mu \geq 0.8$, there is no correlation, Figs. 5f-h.

Figures 6a-g show that the analysis captures the measured H-force trends for $\mu \leq 0.9$, with substantial underprediction at high μ. For $\mu = 1.0$, there is no correlation, Fig. 6h. Both test and analysis show the same linear trend at high μ, μ = 0.6-0.9, Figs. 6d-g. The H-force, the rotor drag in the shaft axes, generally increases with the advance ratio, Figs. 6a-h.

Blade loads and pitch link load

In order to expeditiously assess the overall predictive capability of the current analytical model, only half peak-to-peak loads are considered in this initial study. Azimuthal time histories may be considered in a more detailed, anticipated follow-on study that would most likely focus on specific, limited combinations of μ and C_T/σ.

Figures 7-12 show the half peak-to-peak torsion, flatwise and chordwise blade moments at the mid-span and outboard stations, and Fig. 13 shows the half peak-to-peak pitch link load, all as a function of the thrust coefficient C_T/σ. The measured half peak-to-peak loads were obtained from averaged time-histories. These correlations, for μ = 0.3 to 1.0, are listed as follows:

a) Torsion moment at 0.40C, Figs. 7a-h
b) Torsion moment at 0.80C, Figs. 8a-h
c) Flatwise bending moment at 0.50C, Figs. 9a-h
d) Flatwise bending moment at 0.80C, Figs. 10a-h
e) Chordwise bending moment at 0.40C, Figs. 11a-h
f) Chordwise bending moment at 0.80C, Figs. 12a-h

g) Pitch link load, Figs. 13a-h.

Figures 7a-f and 8a-f show that the analysis captures both mid-span and outboard torsion moment trends for $\mu \leq 0.8$, with substantial underprediction at high μ. For $\mu \geq 0.9$, there is no correlation, Figs. 7g-h and 8g-h.

Figures 9a-f and 10a-f show that the analysis captures both mid-span and outboard flatwise moment trends for $\mu \leq 0.8$, with substantial underprediction at high μ. For $\mu \geq 0.9$, there is no correlation, Figs. 9g-h and Figs 10g-h. At 40%NR, Table 1 and the frequency fan plot, Fig. 1, show that the first and second elastic flatwise-bending modes (Flap 2 and Flap 3, respectively) are spread out and also distant from both the torsion and the first elastic chordwise mode, Chord 2. The latter two modes (torsion and Chord 2) are very close to each other. This suggests that the flatwise behavior may be independent of the other modes, and the substantial underprediction of the flatwise bending moments is somewhat surprising since this underprediction occurs even at lower μ (μ = 0.3-0.4, Figs. 9a-b and Figs. 10a-b). This unexpected difference between the flatwise moment measurements and predictions definitely merits further study. For $\mu \geq 0.9$, there is no correlation, Figs. 9g-h and 10g-h.

Figures 11a-e and 12a-e show that the analysis captures both mid-span and outboard chordwise moment trends for $\mu \leq 0.7$, with substantial underprediction at high μ. Generally, for $\mu \geq 0.8$, there is no correlation, Figs. 11f-h and Figs. 12f-h.

Figures 13a-b show that the measured pitch link load trends are captured by the analysis at low μ; and Figs. 13c-h show that the measured trends are not captured by the analysis for $\mu \geq 0.5$, with the predicted trends totally incorrect at the higher thrust coefficients.

To summarize, overall, the half peak-to-peak blade loads are underpredicted and the half peak-to-peak pitch link load correlation is not good. There is considerable scope for improvement in the prediction of the blade loads.

Comparisons with H-34 correlation

The performance and loads correlations at individual advance ratios have been shown without getting into any detailed discussions. This section contains a limited comparison of the present UH-60A performance correlation with the Ref. 2 H-34 performance correlation. For the cases considered in this paper, the UH-60A rotor rotational speed was kept constant at 40%NR, i.e., the RPM was constant. However, for the H-34 rotor, the high advance ratios were obtained by adjusting both the forward speed and the rotor rotational speed, and it appears that the H-34 (ΩR) varied by almost 50% and its RPM was not kept constant, Ref. 8.

The UH-60A rotor blade is highly twisted and has cambered airfoils whereas the H-34 rotor blade has zero twist and a zero camber airfoil. Broadly, the rotors will have different aerodynamics, and, as identified in Ref. 3, the UH-60A slowed rotor at high advance ratios experiences a unique set of new aeromechanical phenomena.

The comparison with the H-34 correlation is done for the collective pitch = 0^o condition. Figures 14-16 show important performance comparisons with the *advance ratio* μ as the x-axis. The thrust (lift, $\alpha_s = 0^o$), torque, and H-force are considered as follows.

For the thrust (lift), comparing Figs. 14a and 14b, it can be seen that for both UH-60A and H-34, the measured trends are captured by the analysis, but underpredicted.

The torque comparison is shown in Figs. 15a-b. For the UH-60A, there is considerable overprediction, Fig. 15a; for the H-34, the measured trend is captured by the analysis, Fig. 15b. Overall, the H-34 correlation is better.

The H-force comparison is shown in Figs. 16a-b. For the UH-60A, the analysis roughly captures the trend, with considerable underprediction at intermediate advance ratios, Fig. 16a; for the H-34, the measured trend is captured by the analysis and the correlation is good, Fig. 16b. Overall, the H-34 correlation is better.

To summarize, the current, initial UH-60A performance correlation does not seem to be as good as the H-34 correlation, but it must be kept in mind that the H-34 rotor blade is a "simpler" blade, with zero twist and a zero camber airfoil. That is, in the context of the findings of Ref. 3, the UH-60A slowed rotor at high advance ratios presents a more complex, challenging problem that needs further study, and this is discussed as follows.

Analytical model limitations and potential improvements

As noted in the Introduction, this analytical effort is a work in progress. The current modeling assumptions are discussed as follows:

a) The prescribed (rigid) *wake* was used in this study and the more complex free wake models could be used. Reference 9 has shown that compared to the rolled-up wake model, the multiple trailer wake model results in better prediction of the blade chordwise bending moments.

b) At 40%NR, the representative *Reynolds Number* is much smaller than at 100%NR. The Reynolds Number correction was implemented in a limited manner for a single advance ratio μ = 0.6 in this initial study, but these preliminary results (not shown in this paper) were inconsistent and further study is planned.

c) The current model, based on table look up for the airfoil sectional lift, drag and moment data, accounts for *reverse flow*. However, it is not known at present to what extent phenomenon such as "reverse chord dynamic stall,"

Ref. 3, would modify the current UH-60A airfoil tables (that is, without getting into CFD-based computing). Semi-empirical modifications to the airfoil tables may be one approach that can be pursued. Such modifications have been successfully implemented in Ref. 9 for a different rotor system.

d) As noted in the Analytical Model section, the currently used UH-60A *control system stiffness* is based on the flight test article and any differences in the control system stiffness associated with the current wind tunnel configuration have not been accounted for in this study. Considering that the current pitch link load correlation is not good and could be improved, the analytical control system model should be considered in more detail for possible revision.

Finally, plotting both measured and predicted data versus the collective, or μ, instead of C_T/σ will give different insight. At high μ, C_T/σ does not change much with collective so the data tends to go straight up. An anticipated follow-on study will implement this suggestion, but before this is done, the discrepancy noted in the discussion of Fig. 2, the delta between the experimental and analytical collectives, has to be resolved. Perhaps, the advance ratio μ could be used as the independent parameter, the x-axis, e.g., Fig. 14.

Conclusions

The prediction of UH-60A rotor performance and loads at high advance ratio was considered in this analytical study. Measured data from the 40- by 80-Foot Wind Tunnel were compared with CAMRAD II predictions. The emphasis in this initial study was to correlate overall trends. Initial results that represent work in progress were shown and found to be encouraging.

For a rotor rotational speed 40%NR (approximately 104 RPM) and shaft angle $\alpha_s = 0^o$, the complete range of advance ratios, $\mu = 0.3\text{-}1.0$, was considered The rotor performance parameters considered were as follows: thrust coefficient, power coefficient, L/D_E, torque, and H-force. The blade loads considered were as follows: the half peak-to-peak mid-span and outboard torsion, flatwise, and chordwise moments, and the pitch link load.

It was found that for advance ratios ≤ 0.7, the overall trends for the performance and loads (excluding the pitch link load) could be captured, but with substantial overprediction or underprediction. The correlation gradually deteriorated as the advance ratio was increased and for advance ratios ≥ 0.8 there was no correlation. The pitch link load correlation was not good. There is considerable scope for improvement in the prediction of the blade loads.

The limitations of the current analytical model and potential improvements to the model were discussed, for possible implementation in a follow-on study. Considering the modeling complexity associated with the unconventional operating condition under consideration, it is believed that the current predictive ability to capture overall trends is encouraging.

References

1. Norman, T. R., Shinoda, P., Peterson, R. L., and Datta, A., "Full-Scale Wind Tunnel Test of The UH-60A Airloads Rotor," American Helicopter Society Annual Forum 67, May 3-5, Virginia Beach, VA, 2011.

2. Harris, F. D., "Rotor Performance at High Advance Ratio; Theory versus Test," NASA CR 2008-215370, October 2008.

3. Datta, A., Yeo, H., and Norman, T. R., "Experimental Investigation and Fundamental Understanding of a Slowed UH-60A Rotor at High Advance Ratios," American Helicopter Society 67th Annual Forum, Virginia Beach, VA, May 2011.

4. Johnson, W. "CAMRAD II, Comprehensive Analytical Model of Rotorcraft Aerodynamics and Dynamics," Johnson Aeronautics, Palo Alto, California, 1992-1999.

5. Johnson, W. "Technology Drivers in the Development of CAMRAD II," American Helicopter Society, American Helicopter Society Aeromechanics Specialists Conference, San Francisco, CA, January 19-21, 1994.

6. Johnson, W. "A General Free Wake Geometry Calculation for Wings and Rotors," American Helicopter Society 51st Annual Forum Proceedings, Ft. Worth, TX, May 9-11, 1995.

7. Yeo, H., Bousman, W.G., and Johnson, W., "Performance Analysis of a Utility Helicopter with Standard and Advanced Rotor," *Journal of the American Helicopter Society*, Vol. 49, No. 3, July 2004, pp. 250–270.

8. McCloud III, John L., Biggers, James C., and Stroub, R.H, "An Investigation of Full-Scale Helicopter Rotors at High Advance Ratios and Advancing Tip Mach Numbers," NASA TN D-4632, 1968.

9. Kottapalli, S. "Enhanced Correlation of SMART Active Flap Rotor Loads," American Institute of Aeronautics and Astronautics 52nd AIAA/ASME/ASCE/AHS/ASC Structures, Structural Dynamics, and Materials Conference, Denver, CO, April 4-7, 2011, AIAA 2011-1874.

Table 1. Calculated UH-60A rotor blade frequencies, 40%NR.

Blade Mode	Frequency (per rev)
Chord 1	0.32
Flap 1	1.05
Flap 2	3.32
Flap 3	7.33
Chord 2	10.58
Torsion 1	11.20

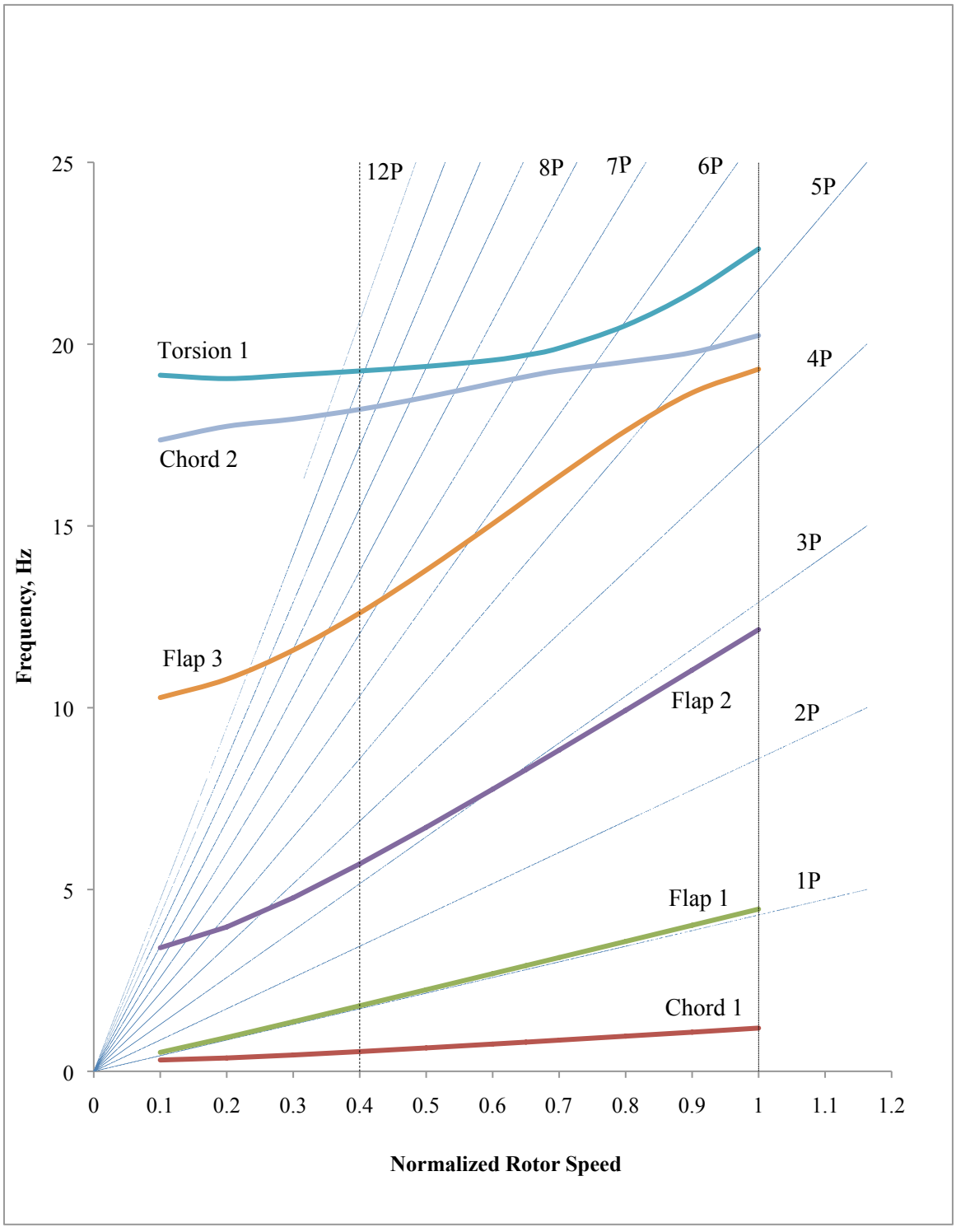

Fig. 1. UH-60A rotor fan plot.

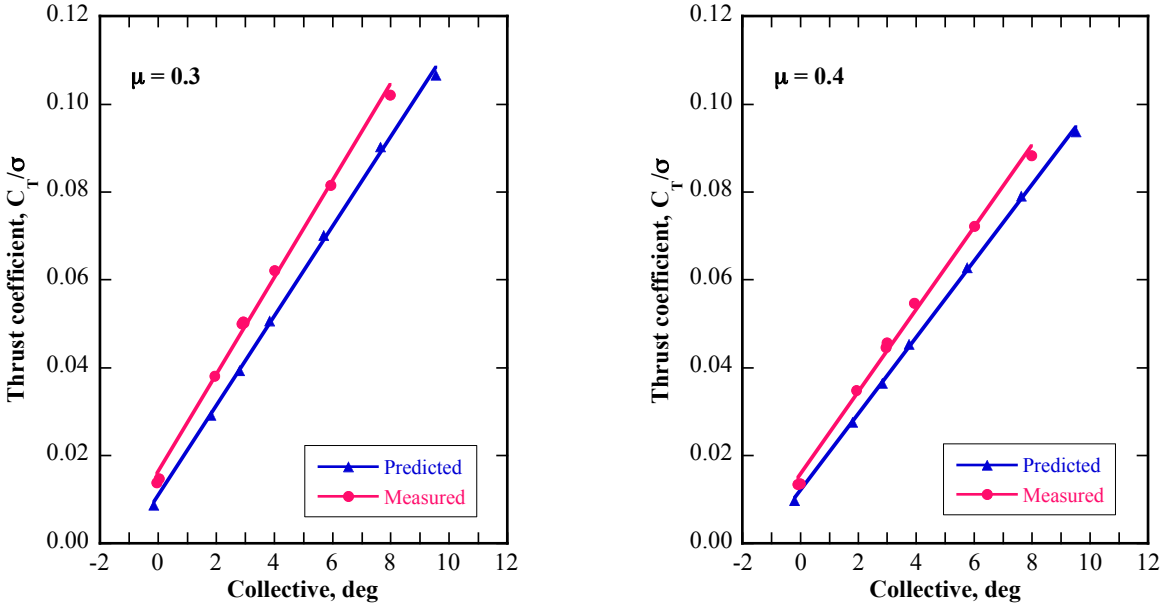

(a)

(b)

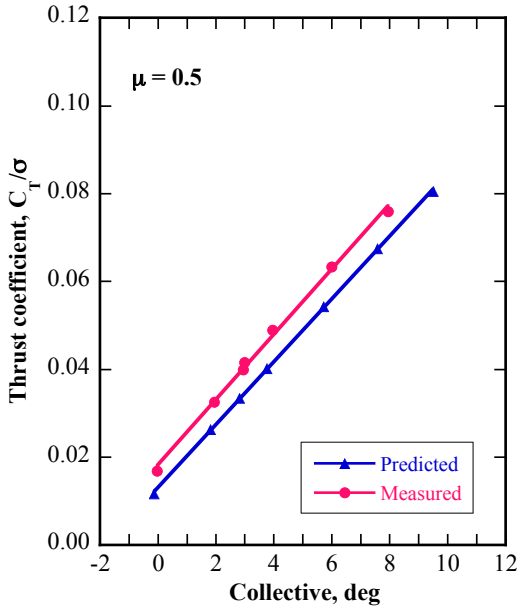

(c)

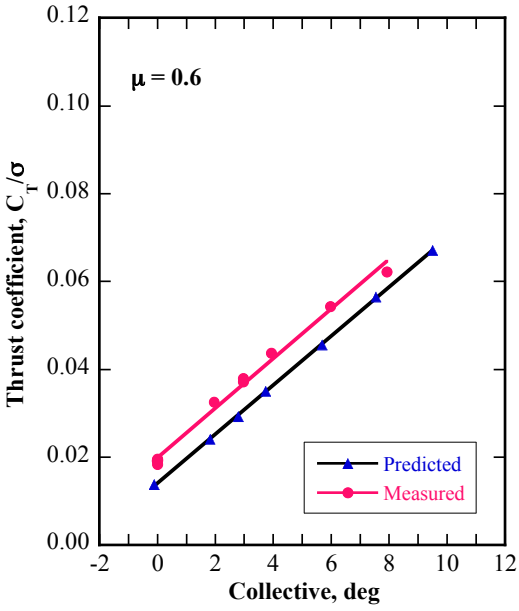

(d)

Fig. 2. Thrust coefficient correlation, $\alpha_s = 0^o$, 40%NR.

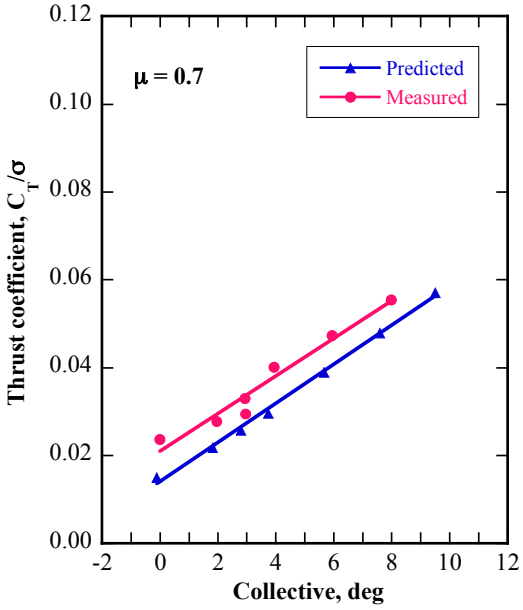

(e)

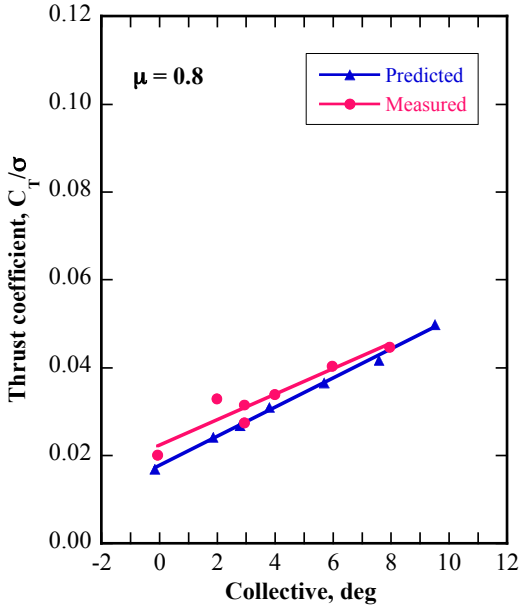

(f)

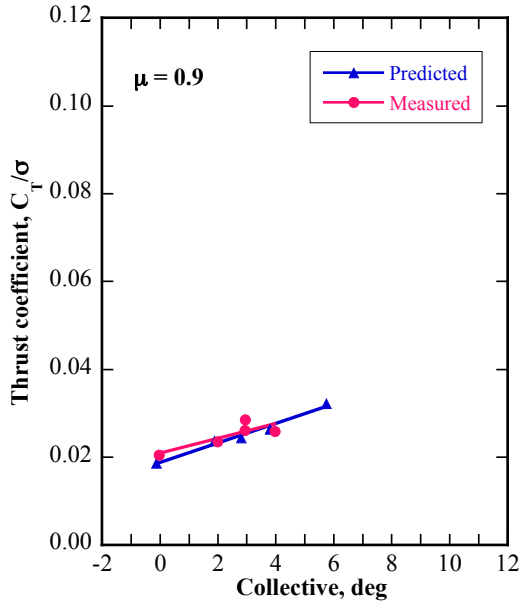

(g)

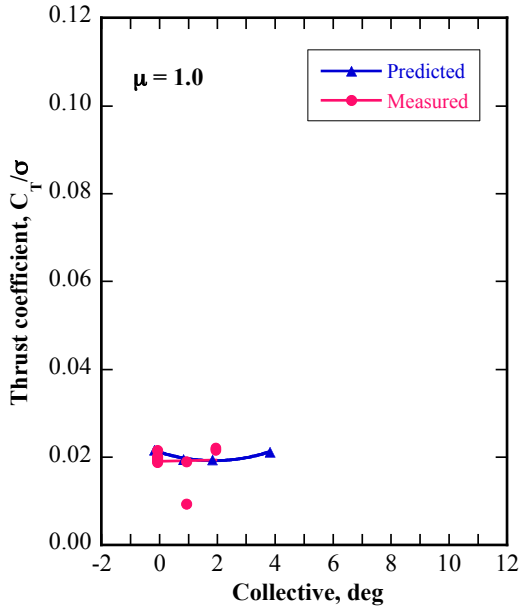

(h)

Fig. 2. cont'd, Thrust coefficient correlation, $\alpha_s = 0^o$, 40%NR.

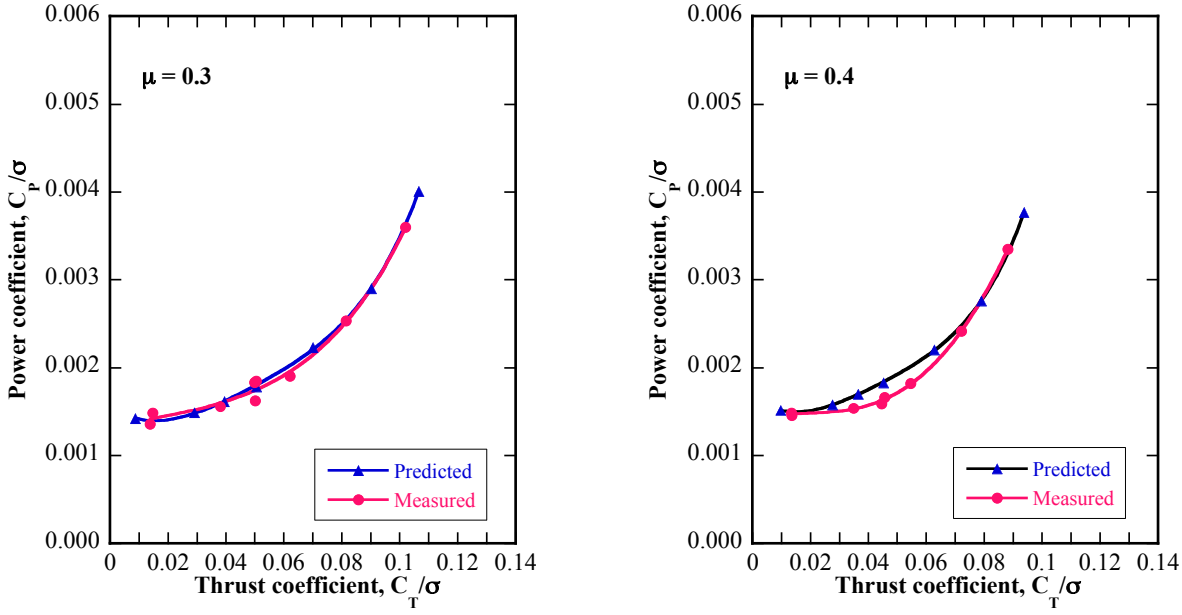

(a)

(b)

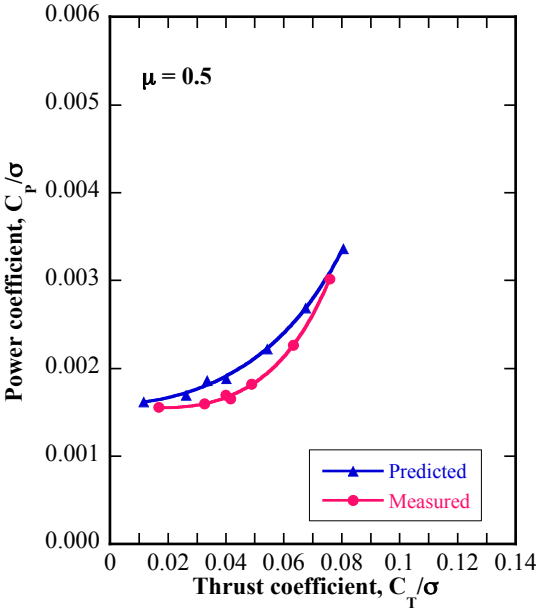

(c)

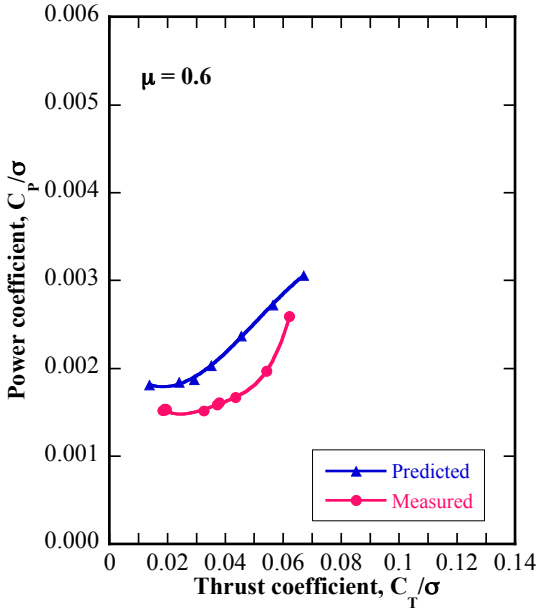

(d)

Fig. 3. Power coefficient correlation, $\alpha_s = 0^o$, 40%NR.

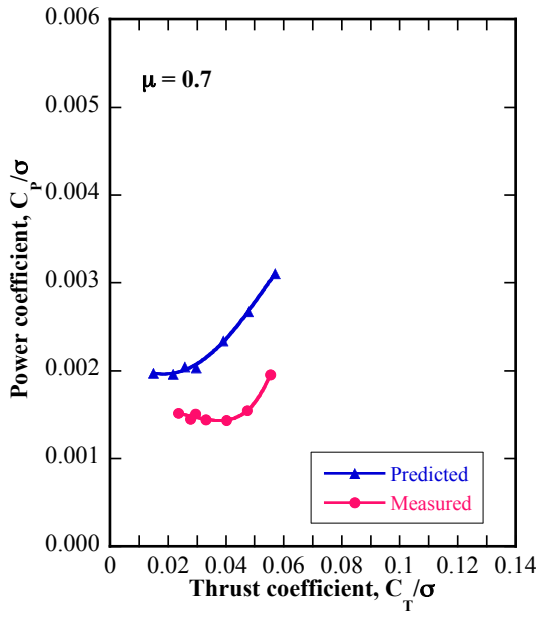

(e)

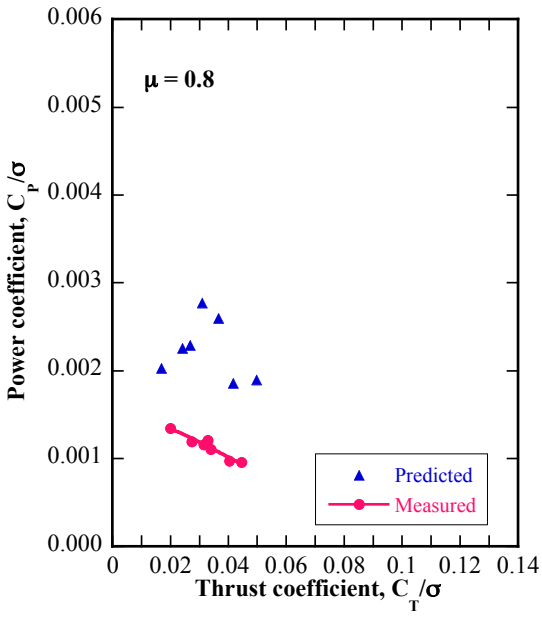

(f)

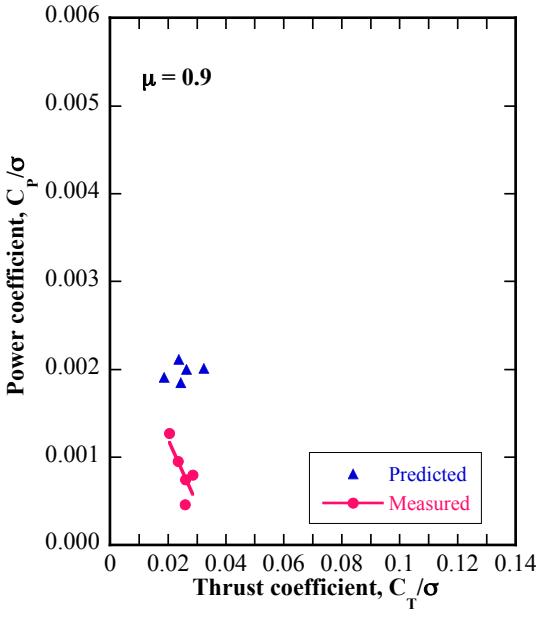

(g)

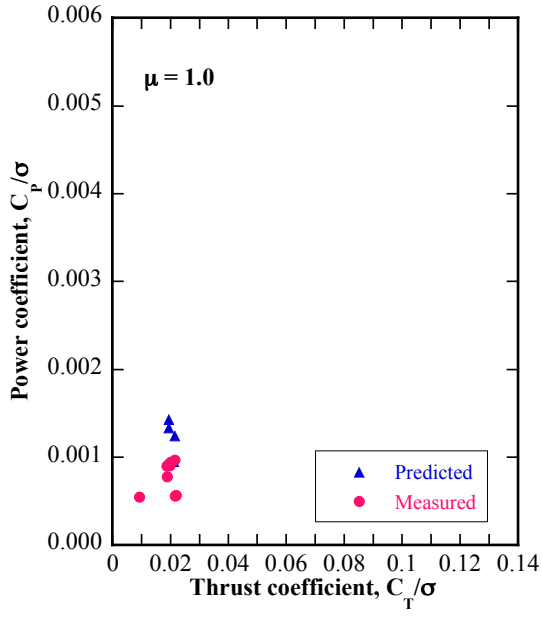

(h)

Fig. 3. cont'd, Power coefficient correlation, $\alpha_s = 0^o$, 40%NR.

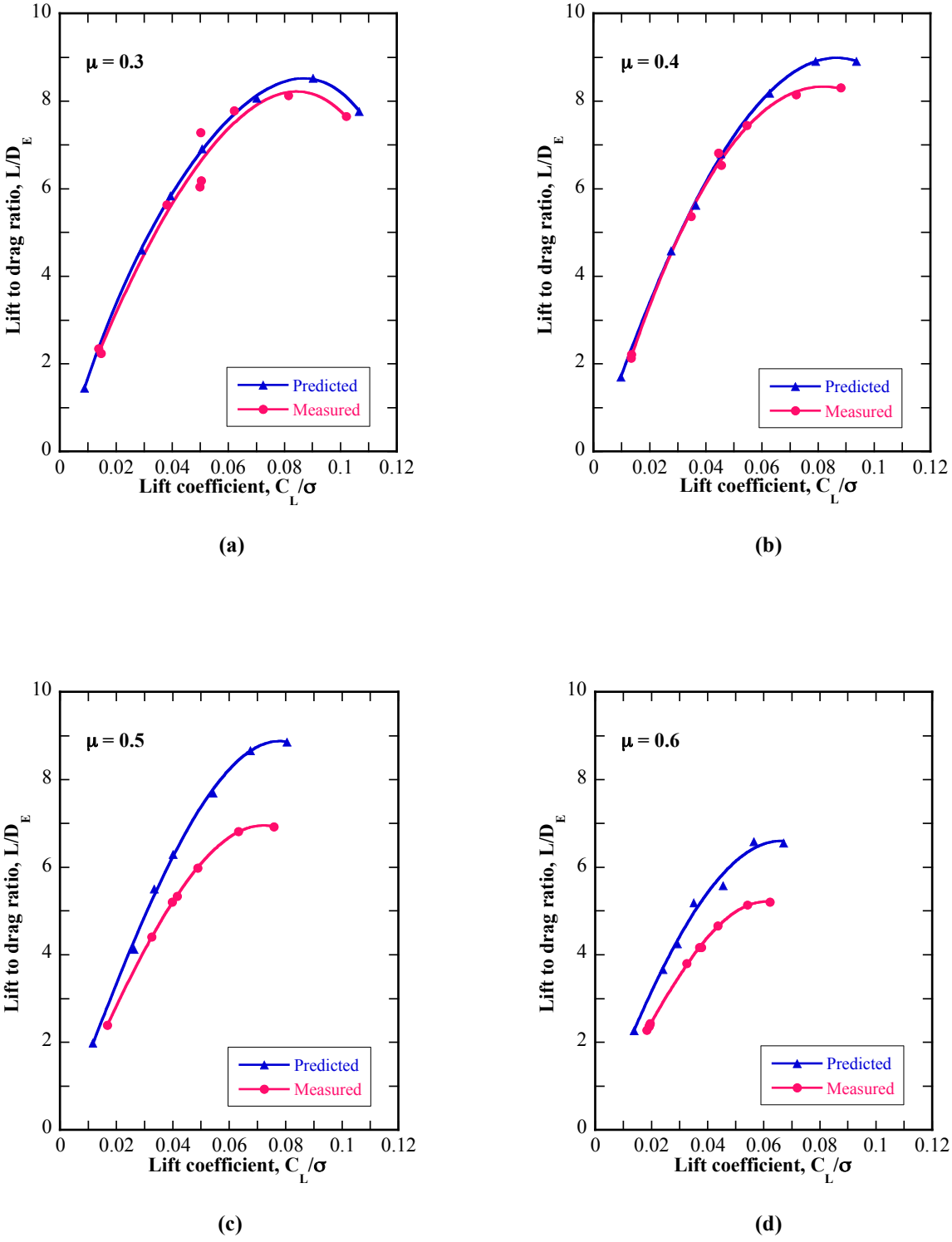

Fig. 4. Lift to drag ratio correlation, $\alpha_s = 0^o$, 40%NR.

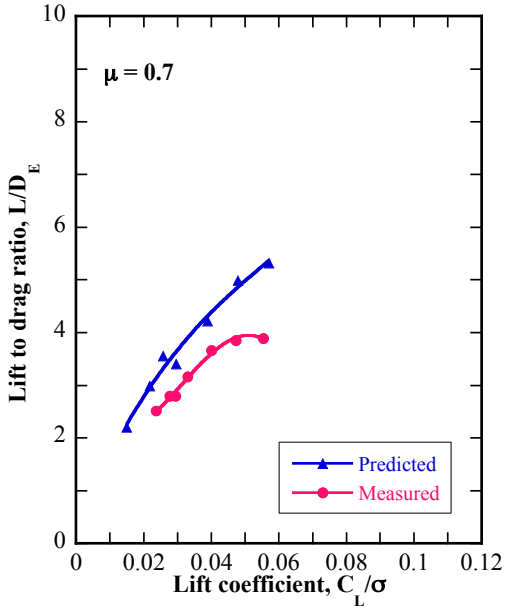

(e)

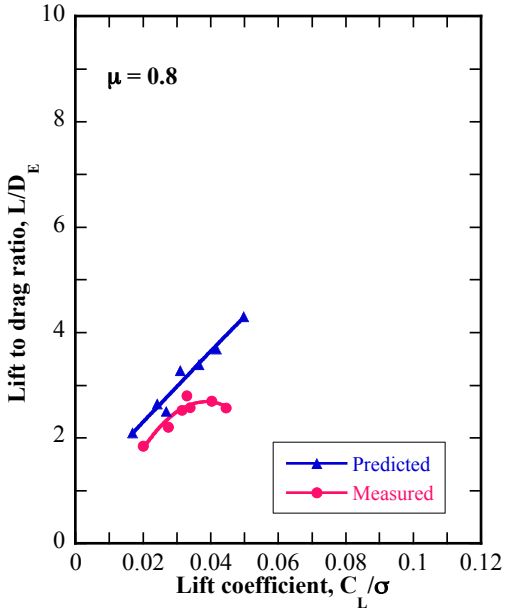

(f)

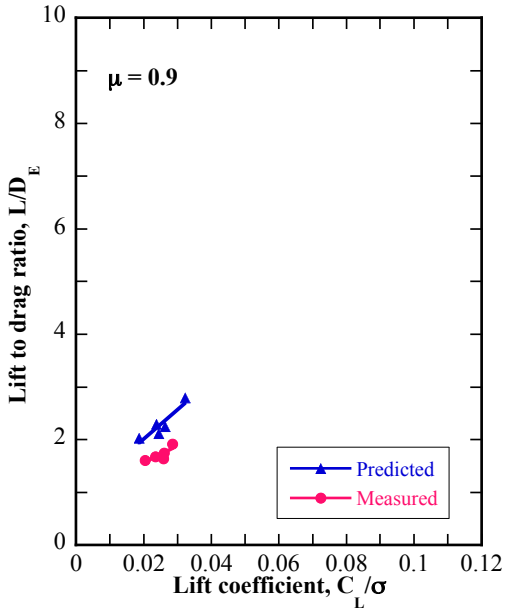

(g)

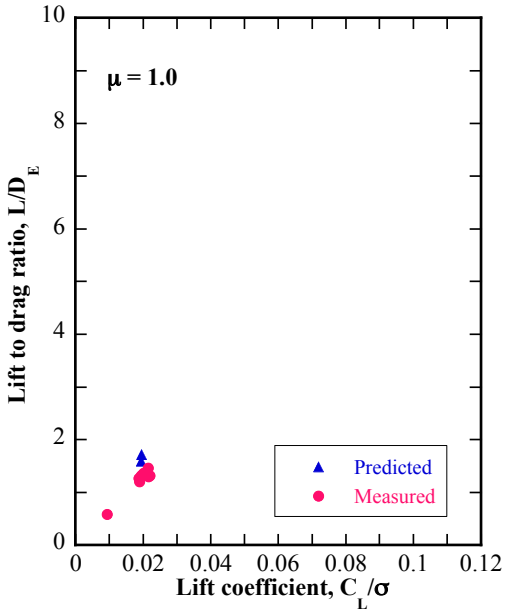

(h)

Fig. 4. cont'd, Lift to drag ratio correlation, $\alpha_s = 0^o$, 40%NR.

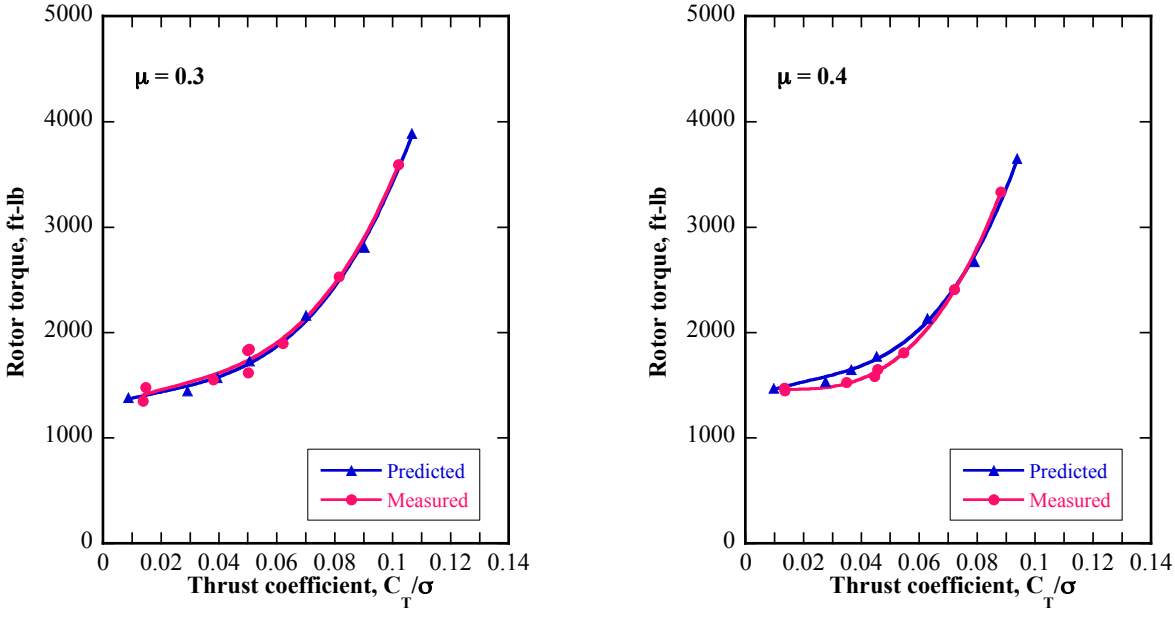

(a)

(b)

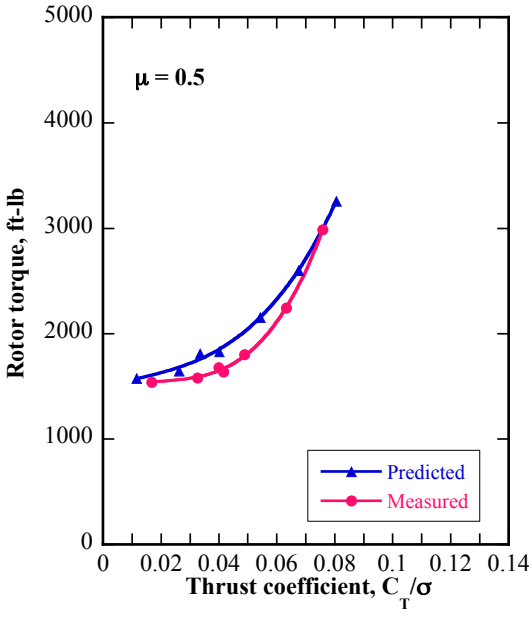

(c)

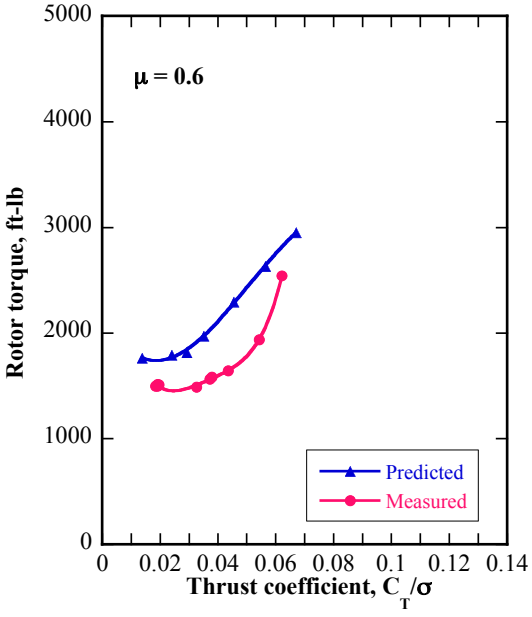

(d)

Fig. 5. Rotor torque correlation, $\alpha_s = 0^o$, 40%NR.

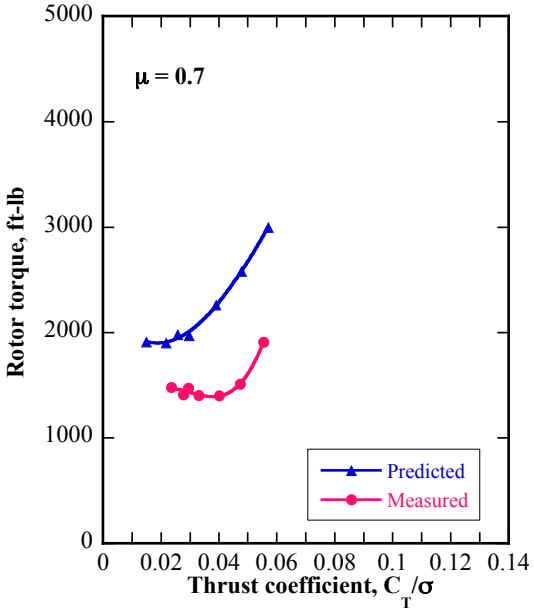

(e)

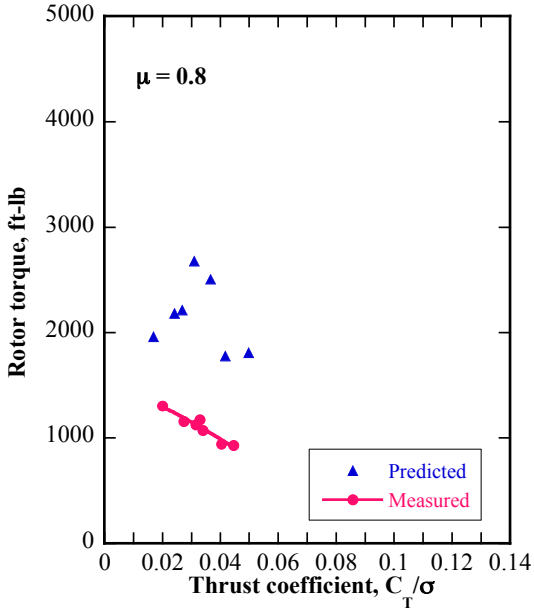

(f)

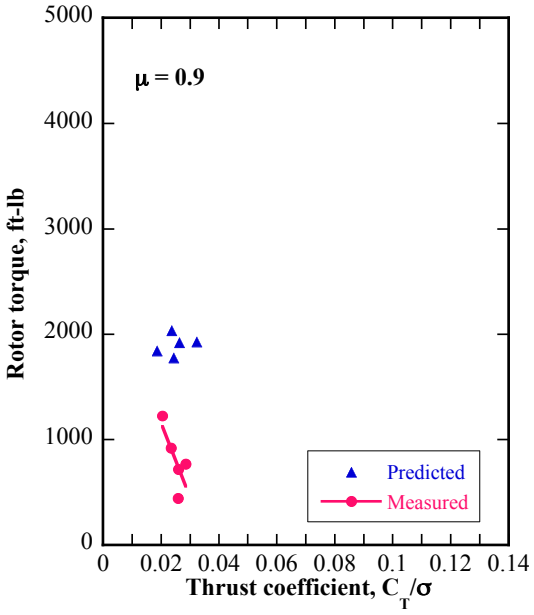

(g)

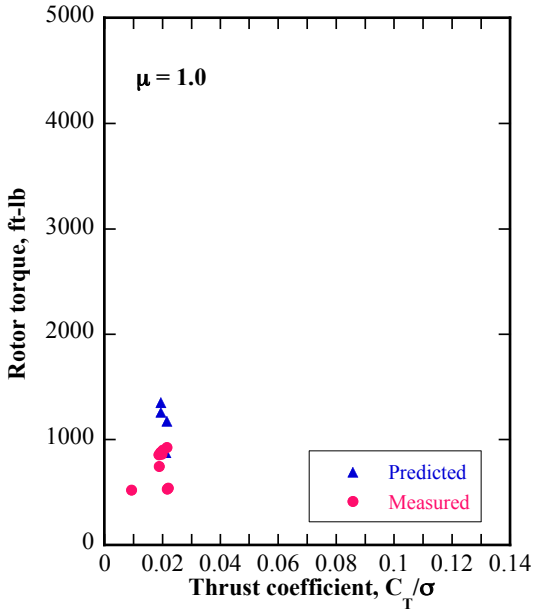

(h)

Fig. 5. cont'd, Rotor torque correlation, $\alpha_s = 0^o$, 40%NR.

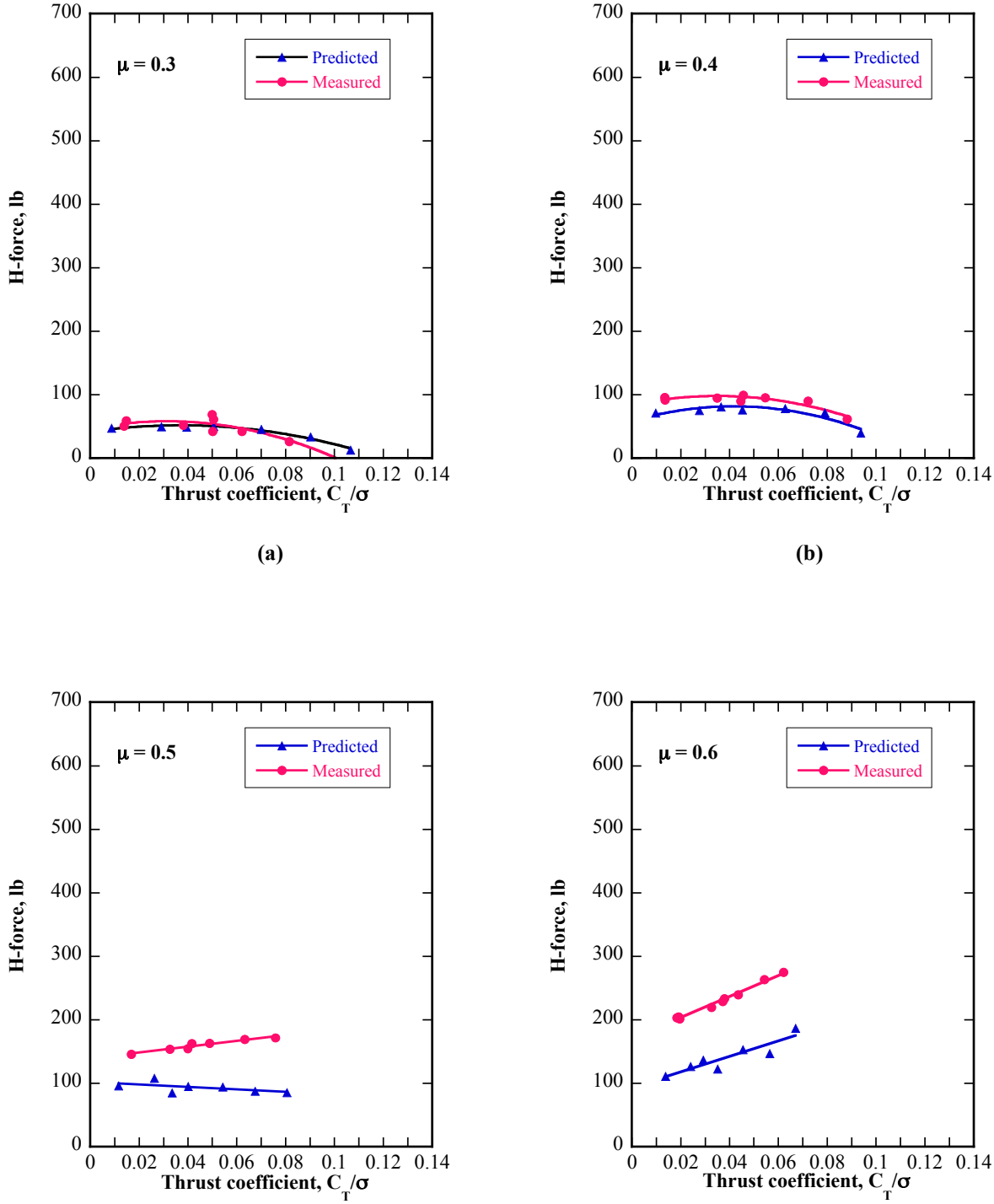

Fig. 6. H-force correlation, $\alpha_s = 0^o$, 40%NR.

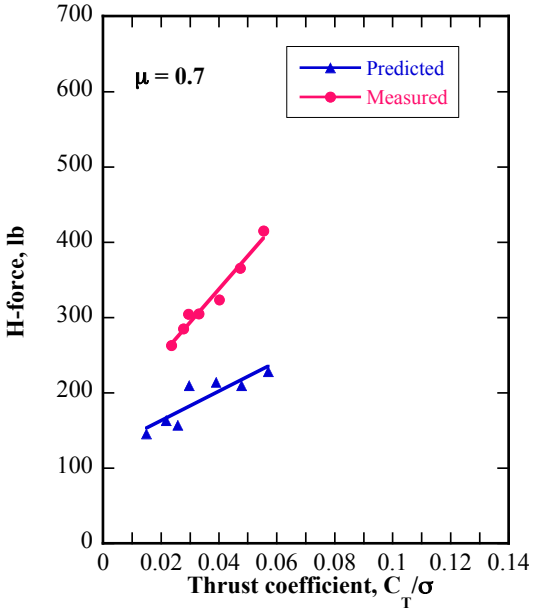

(e)

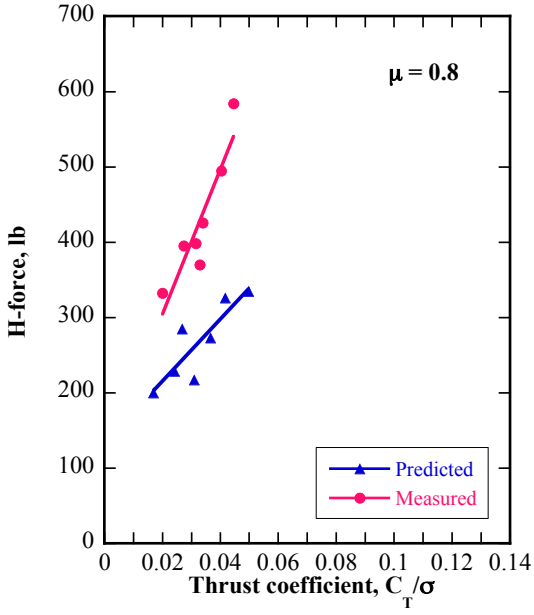

(f)

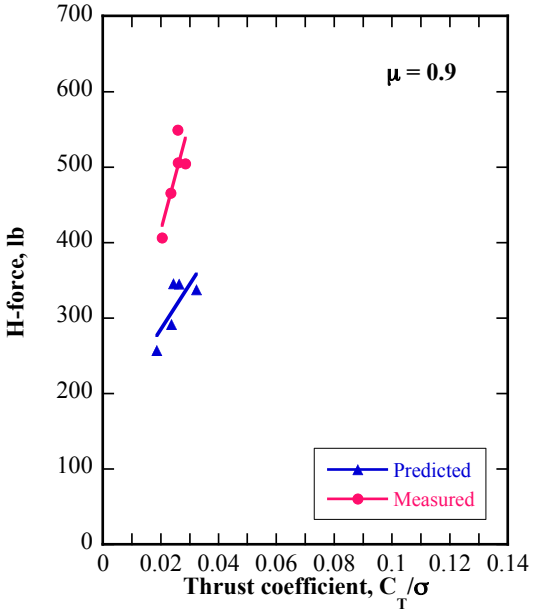

(g)

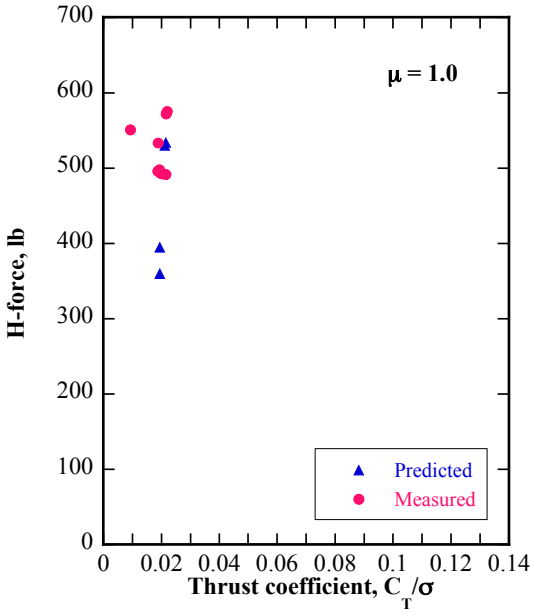

(h)

Fig. 6. cont'd, H-force correlation, α_s = 0°, 40%NR.

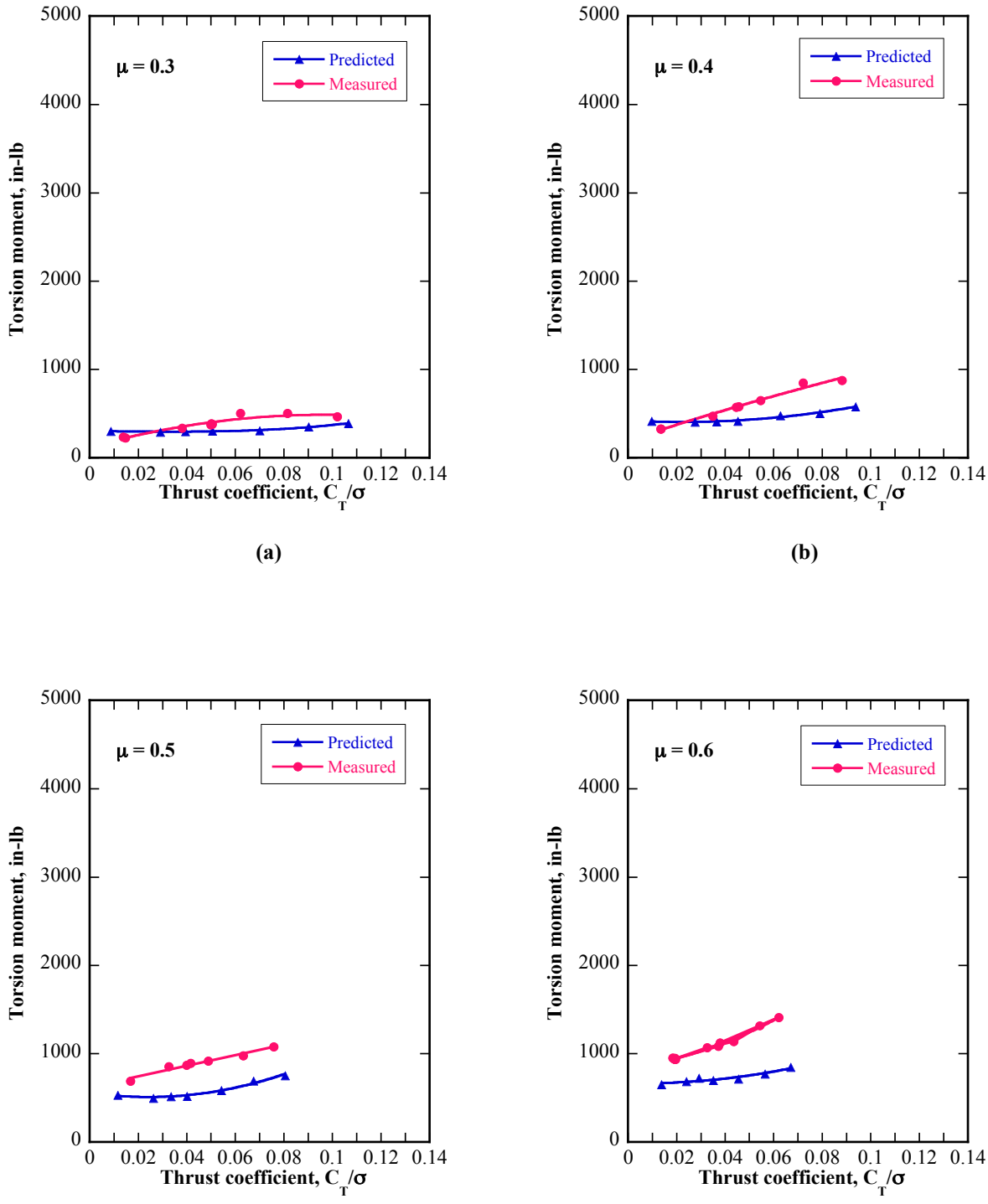

Fig. 7. Half peak-to-peak torsion moment correlation at 0.40R, $\alpha_s = 0^o$, 40%NR.

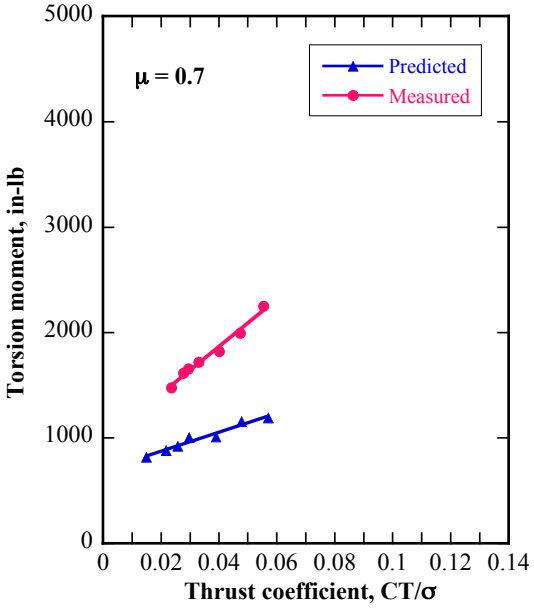

(e)

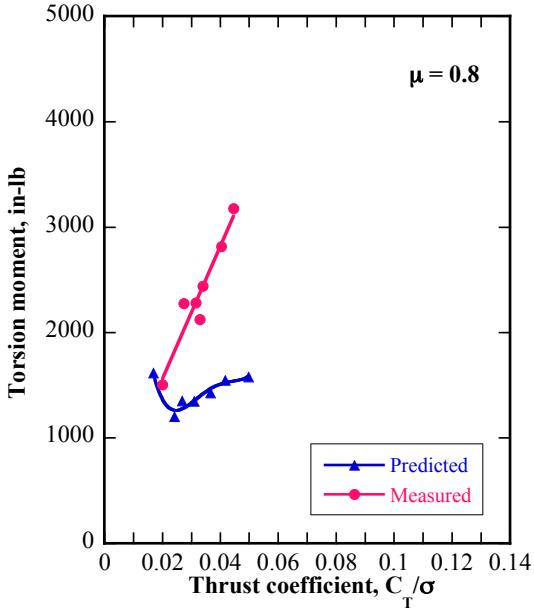

(f)

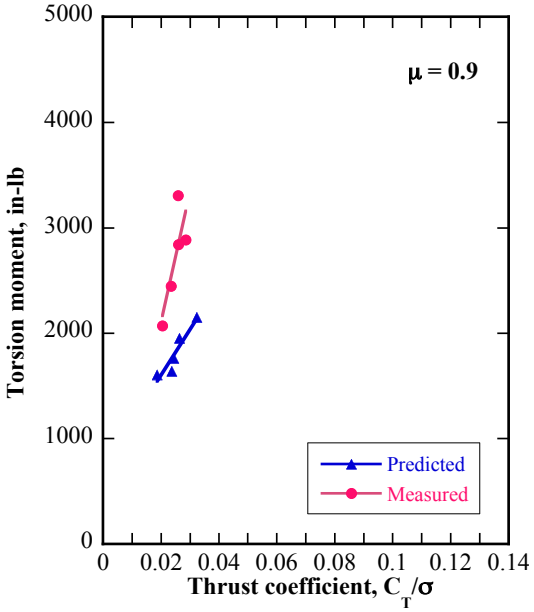

(g)

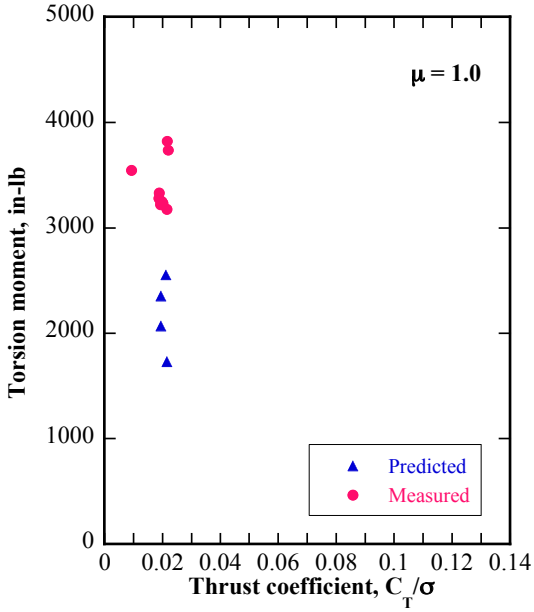

(h)

Fig. 7. cont'd, Half peak-to-peak torsion moment correlation at 0.40R, α_s = 0°, 40%NR.

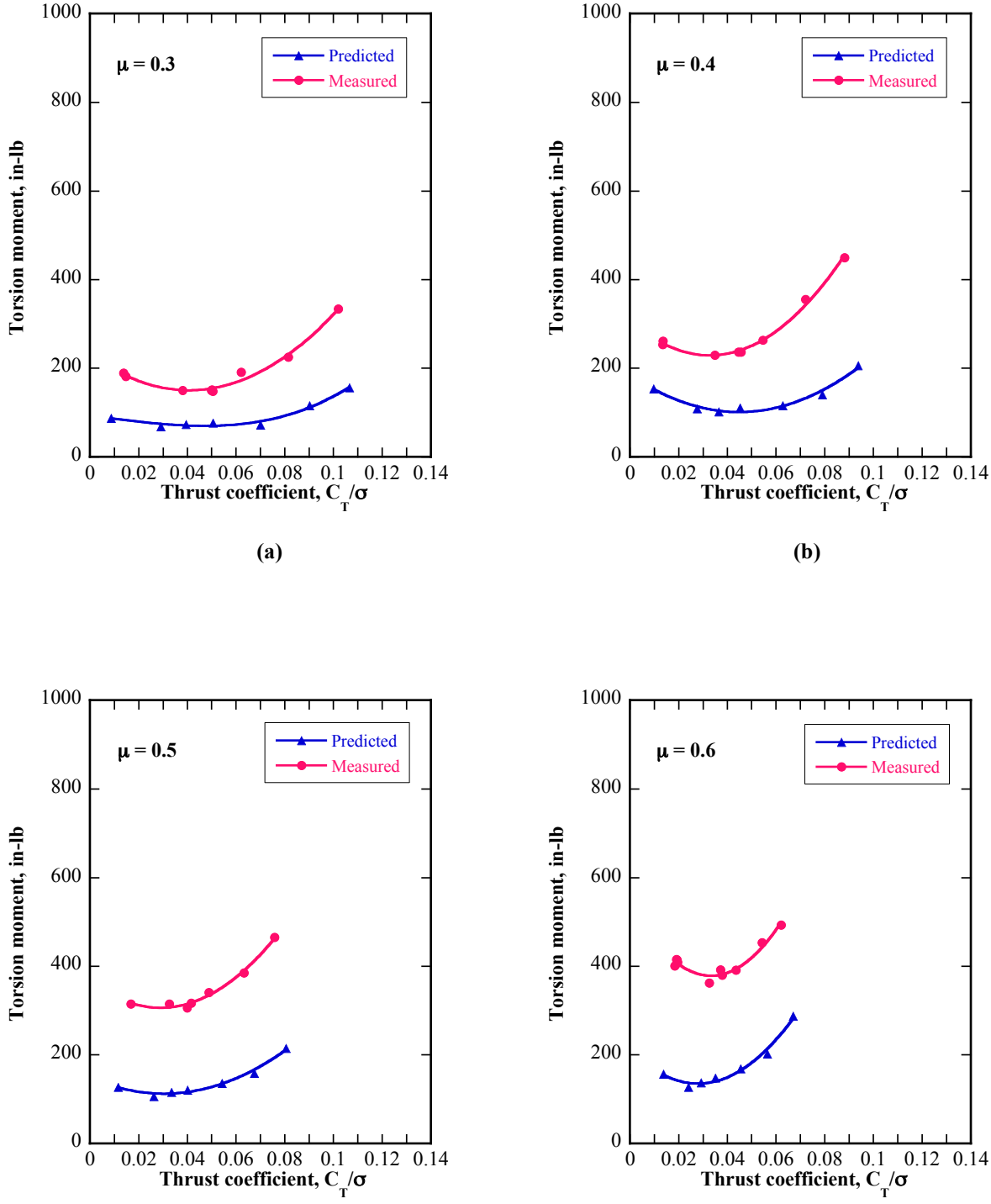

Fig. 8. Half peak-to-peak torsion moment correlation at 0.80R, α_s = 0°, 40%NR.

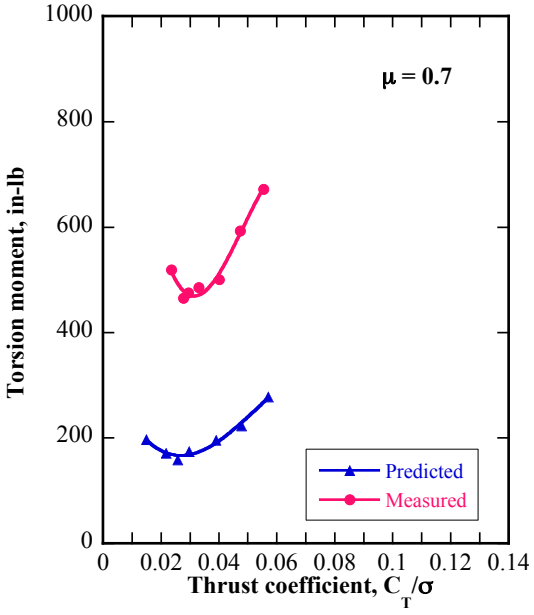

(e)

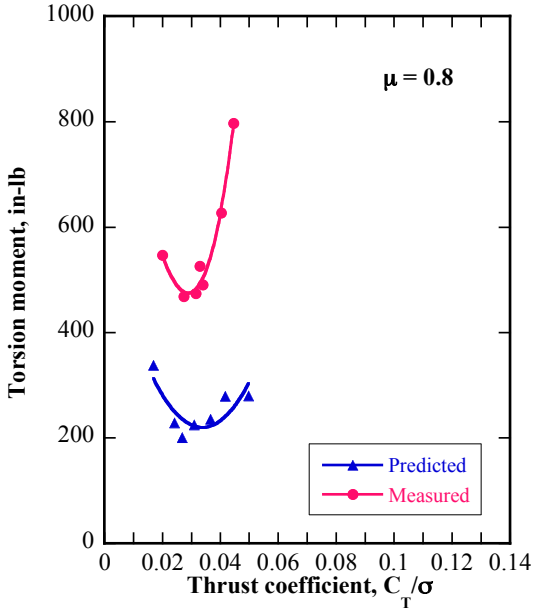

(f)

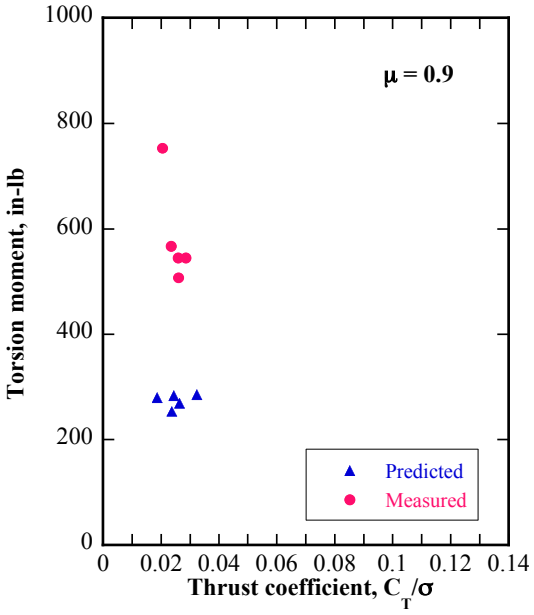

(g)

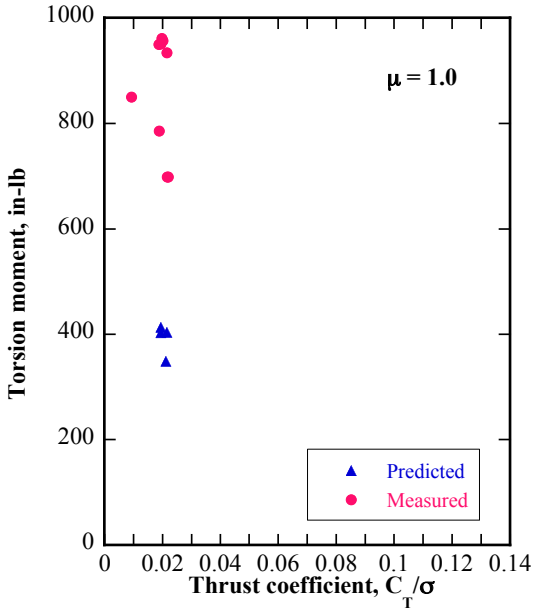

(h)

Fig. 8. cont'd, Half peak-to-peak torsion moment correlation at 0.80R, $\alpha_s = 0^o$, 40%NR.

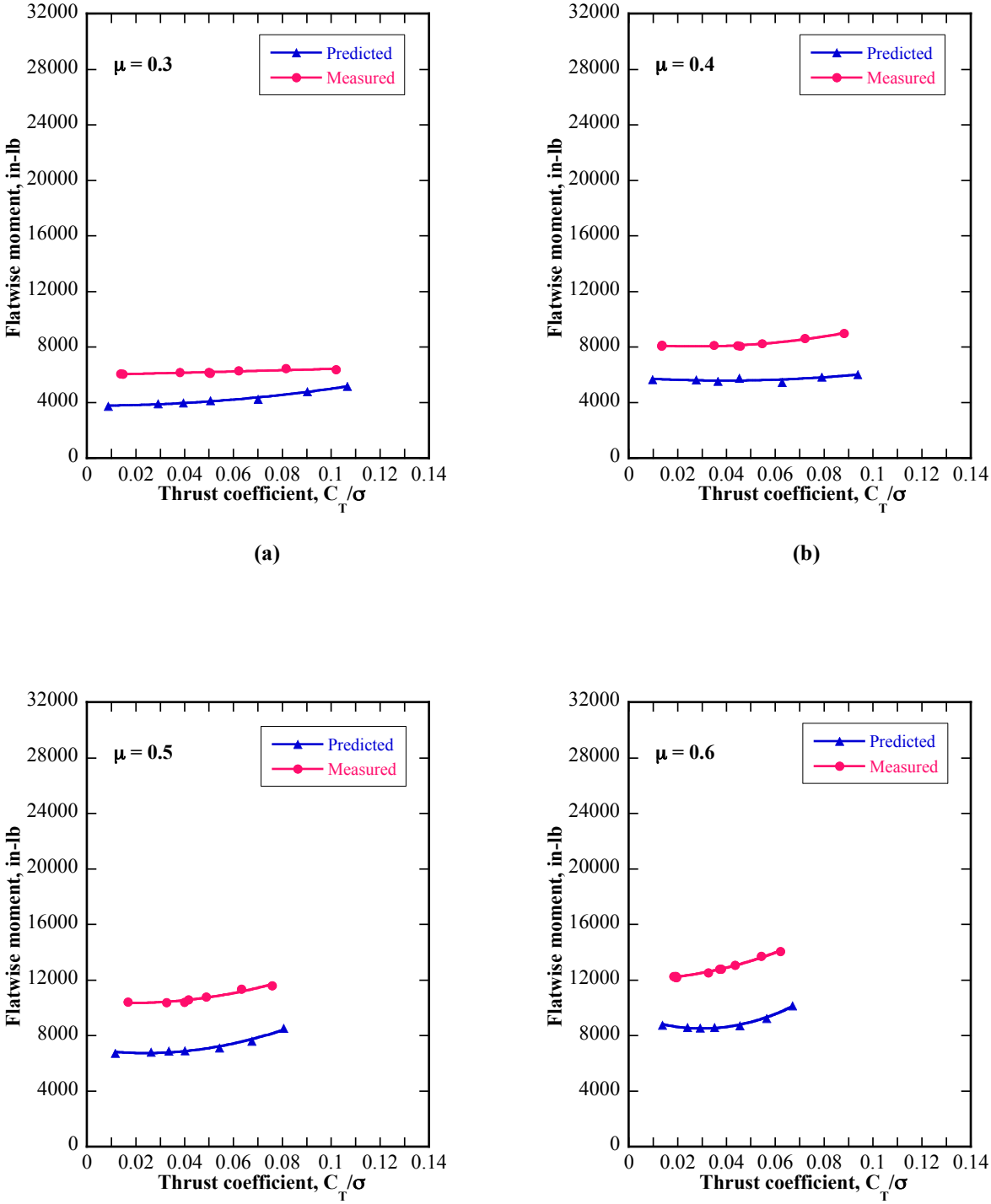

Fig. 9. Half peak-to-peak flatwise moment correlation at 0.50R, α_s = 0°, 40%NR.

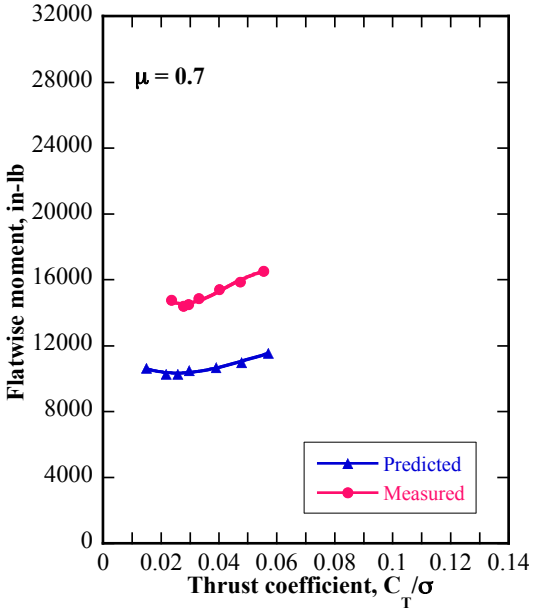

(e)

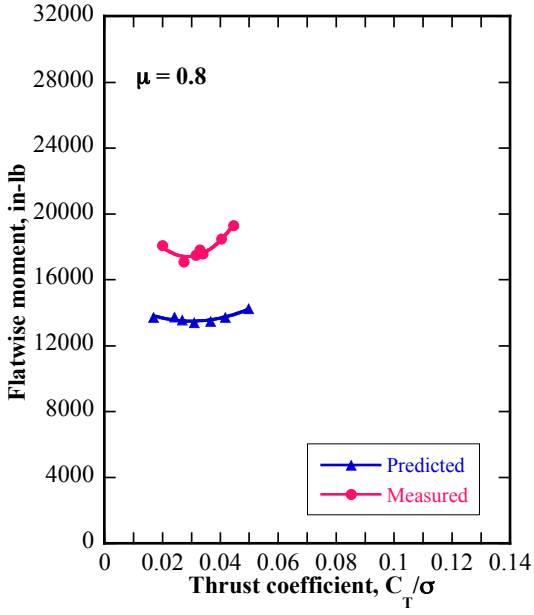

(f)

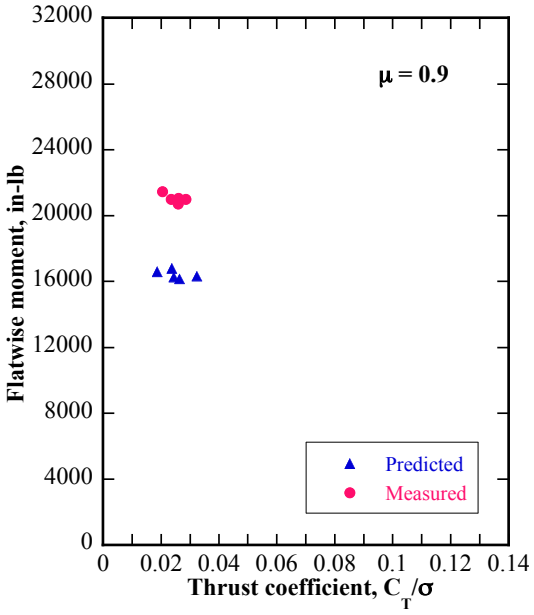

(g)

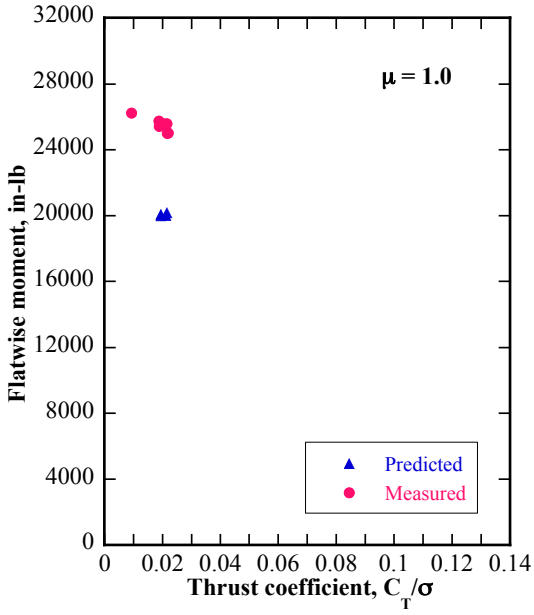

(h)

Fig. 9. cont'd, Half peak-to-peak flatwise moment correlation at 0.50R, α_s = 0°, 40%NR.

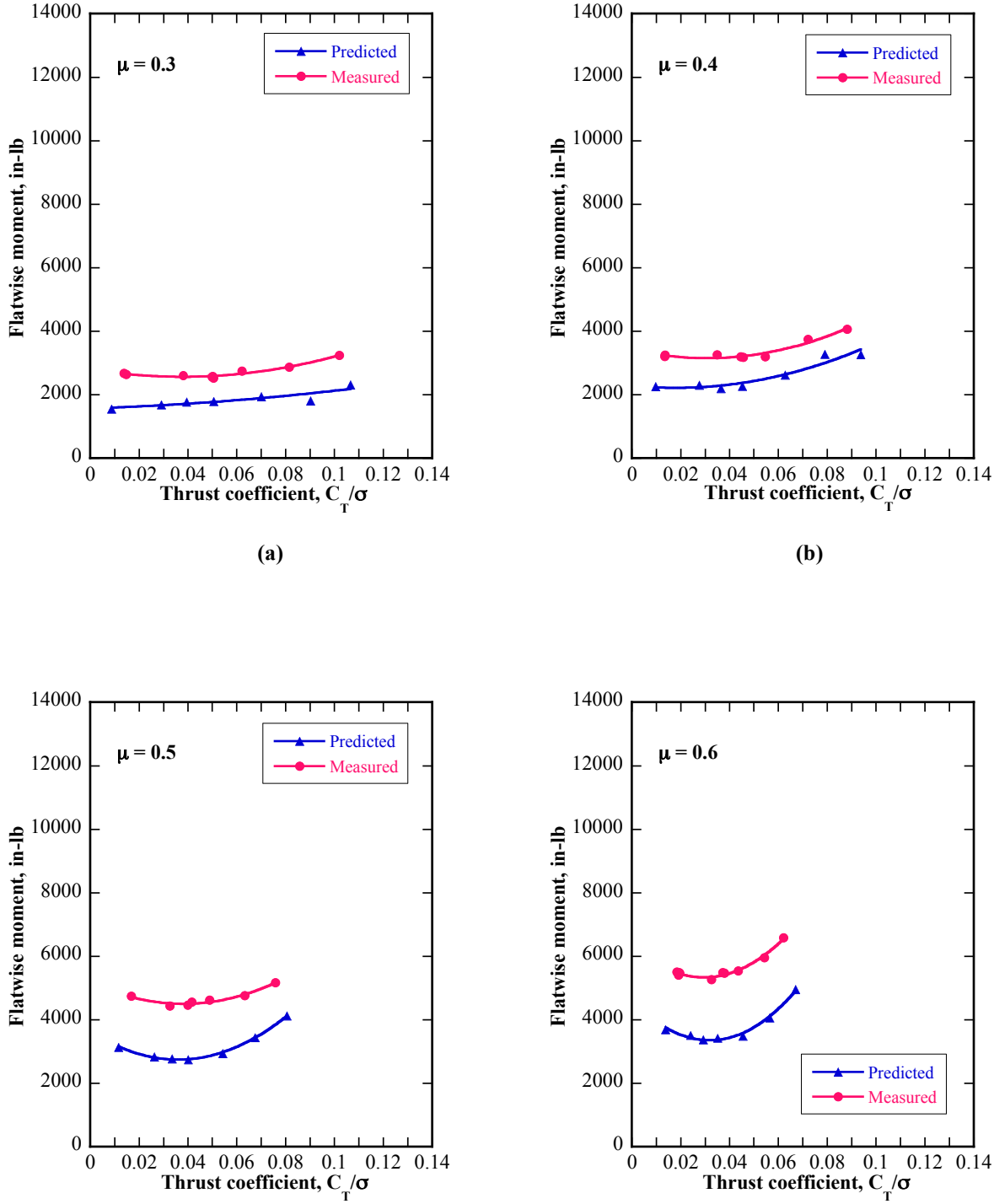

Fig. 10. Half peak-to-peak flatwise moment correlation at 0.80R, α_s = 0°, 40%NR.

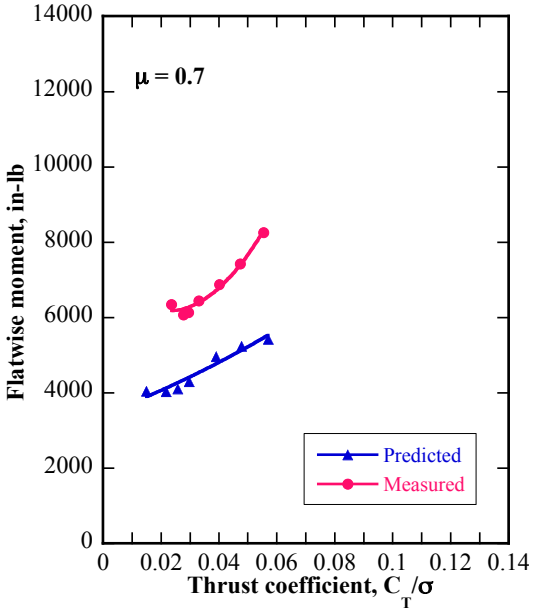

(e)

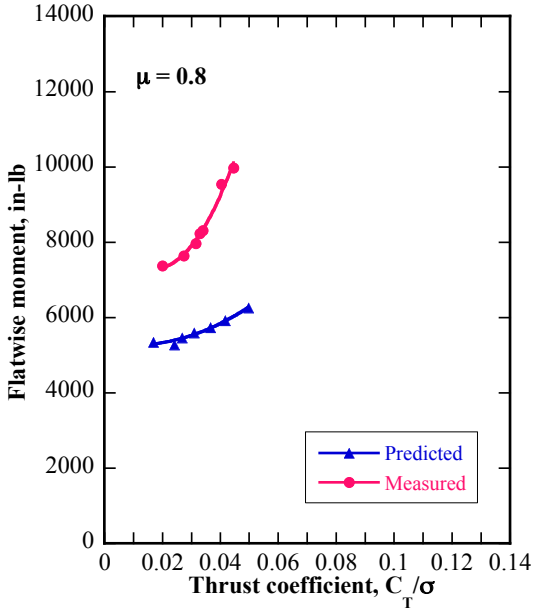

(f)

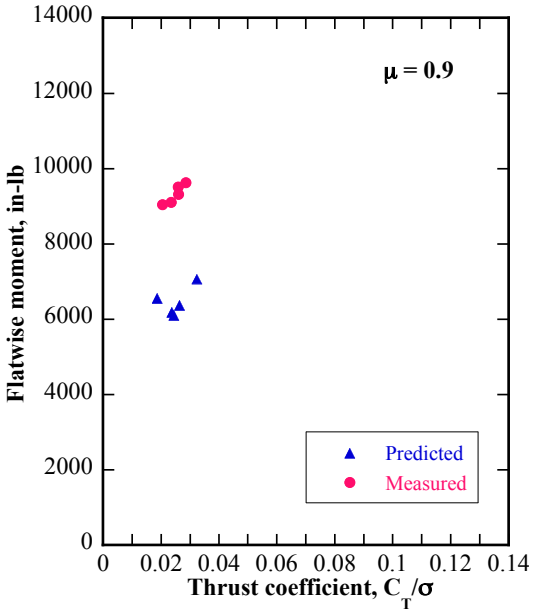

(g)

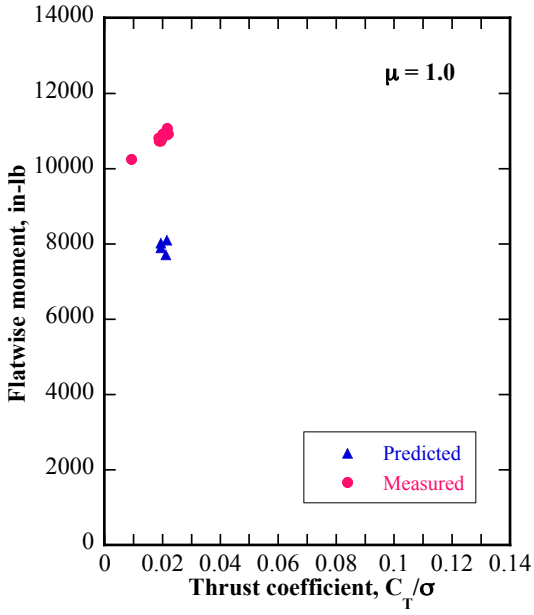

(h)

Fig. 10. cont'd, Half peak-to-peak flatwise moment correlation at 0.80R, α_s = 0°, 40%NR.

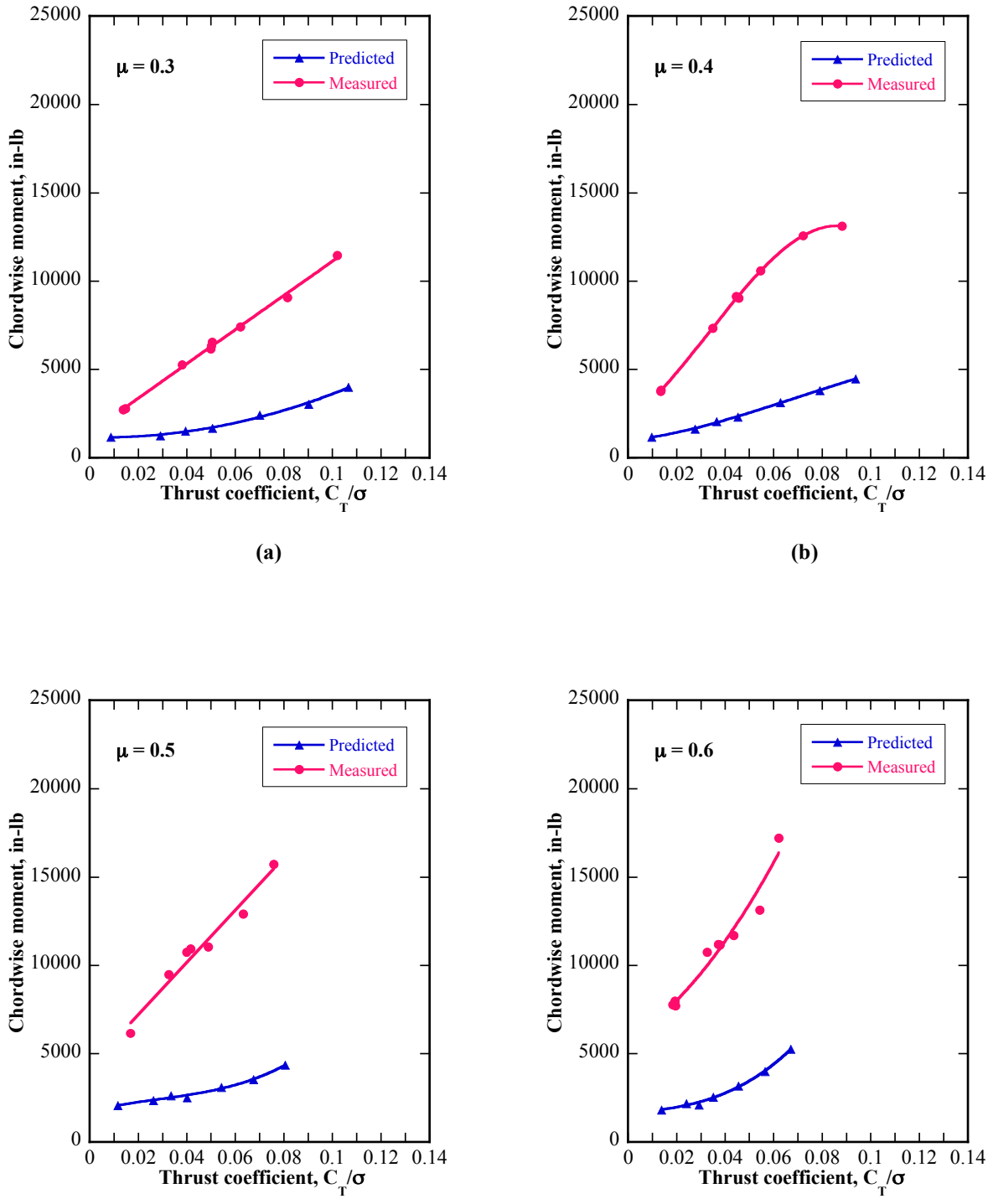

Fig. 11. Half peak-to-peak chordwise moment correlation at 0.40R, $\alpha_s = 0^o$, 40%NR.

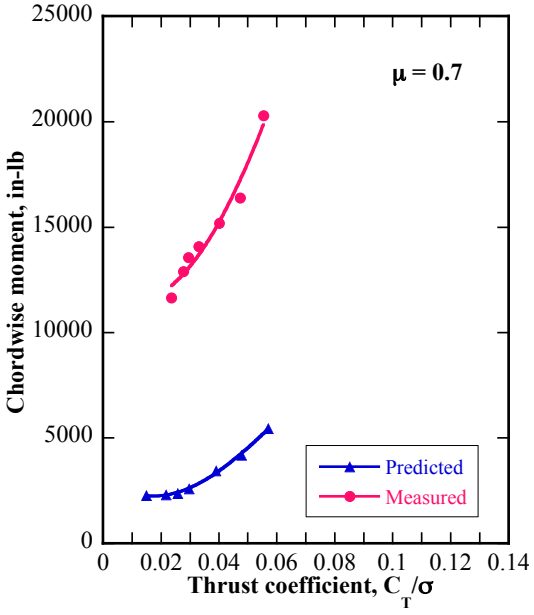

(e)

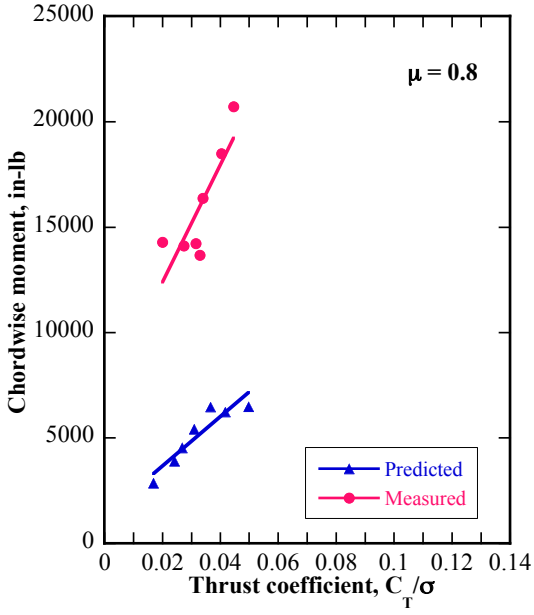

(f)

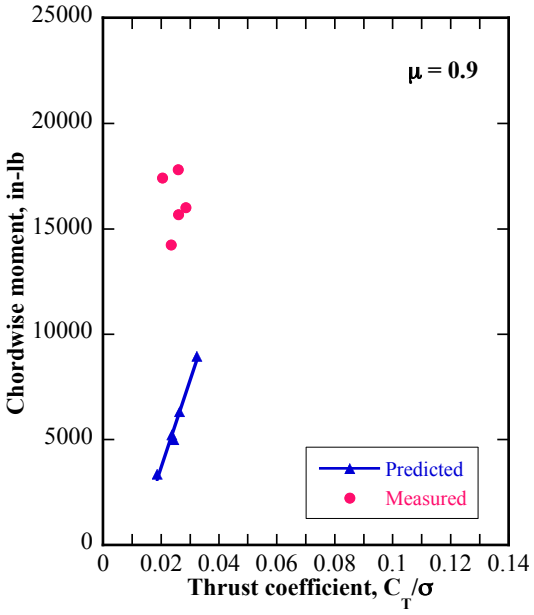

(g)

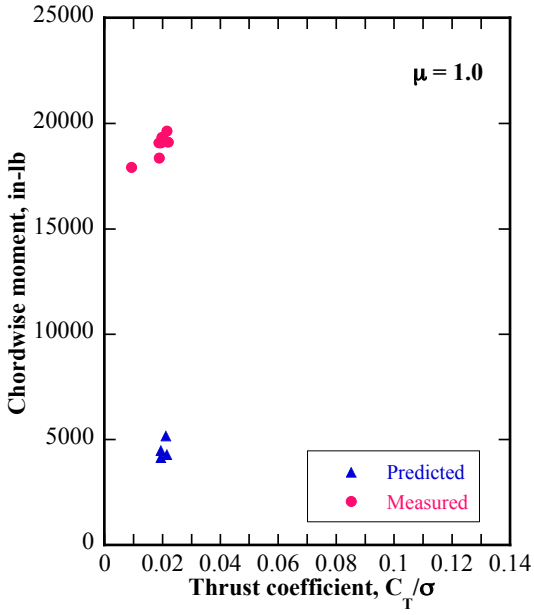

(h)

Fig. 11. cont'd, Half peak-to-peak chordwise moment correlation at 0.40R, $\alpha_s = 0^o$, 40%NR.

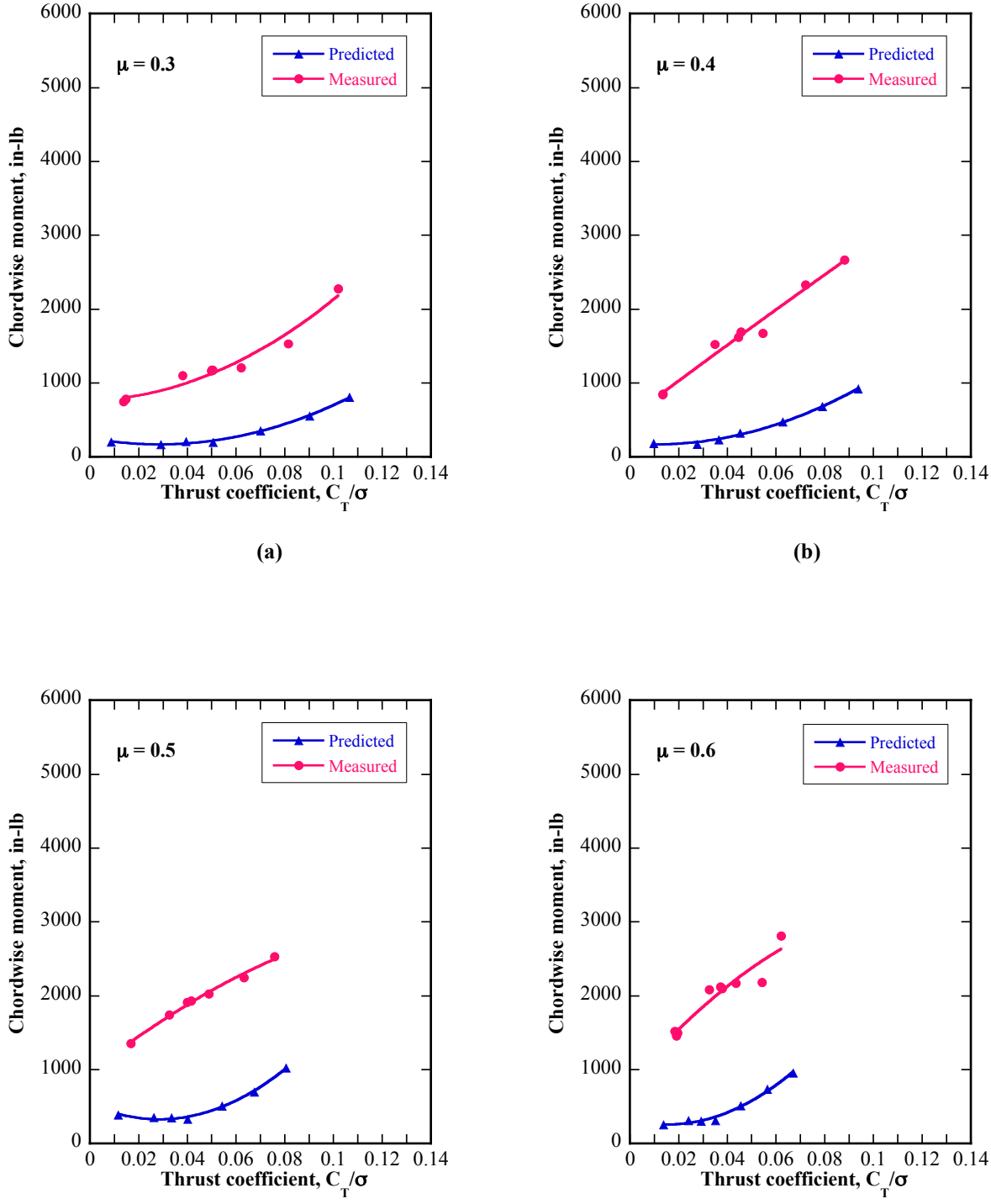

Fig. 12. Half peak-to-peak chordwise moment correlation at 0.80R, α_s = 0°, 40%NR.

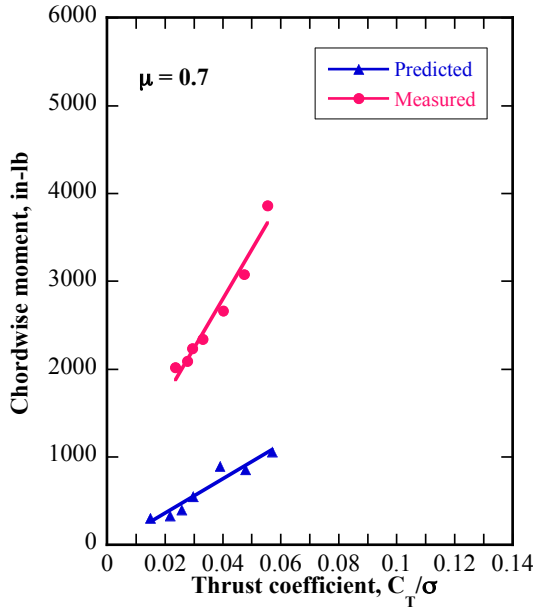

(e)

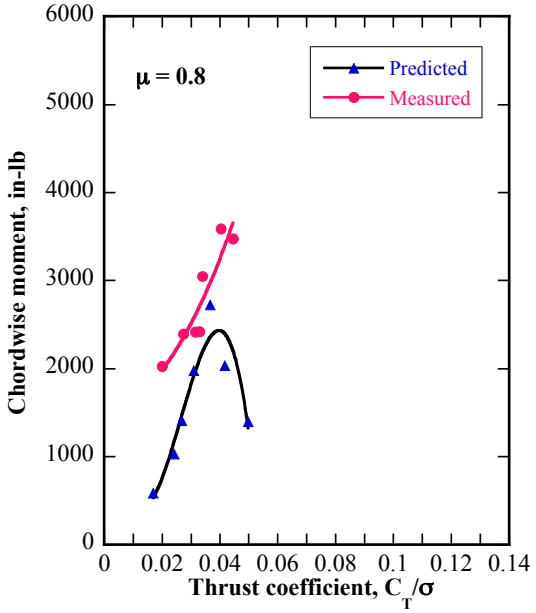

(f)

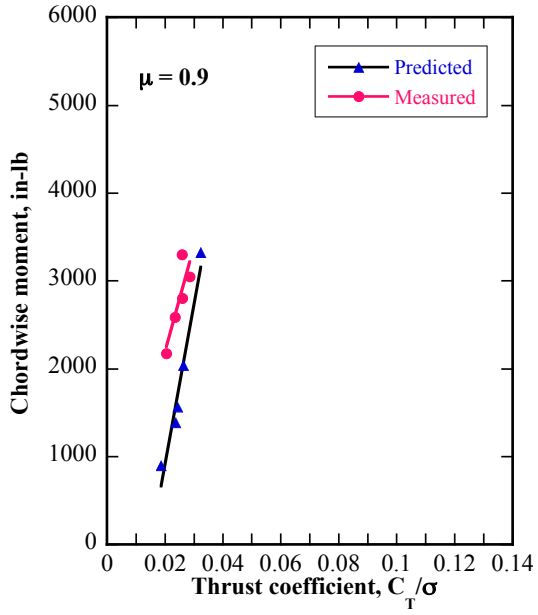

(g)

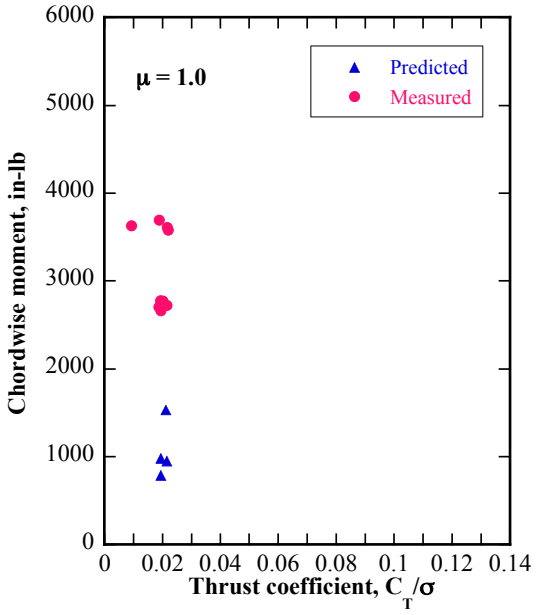

(h)

Fig. 12. cont'd, Half peak-to-peak chordwise moment correlation at 0.80R, α_s = 0°, 40%NR.

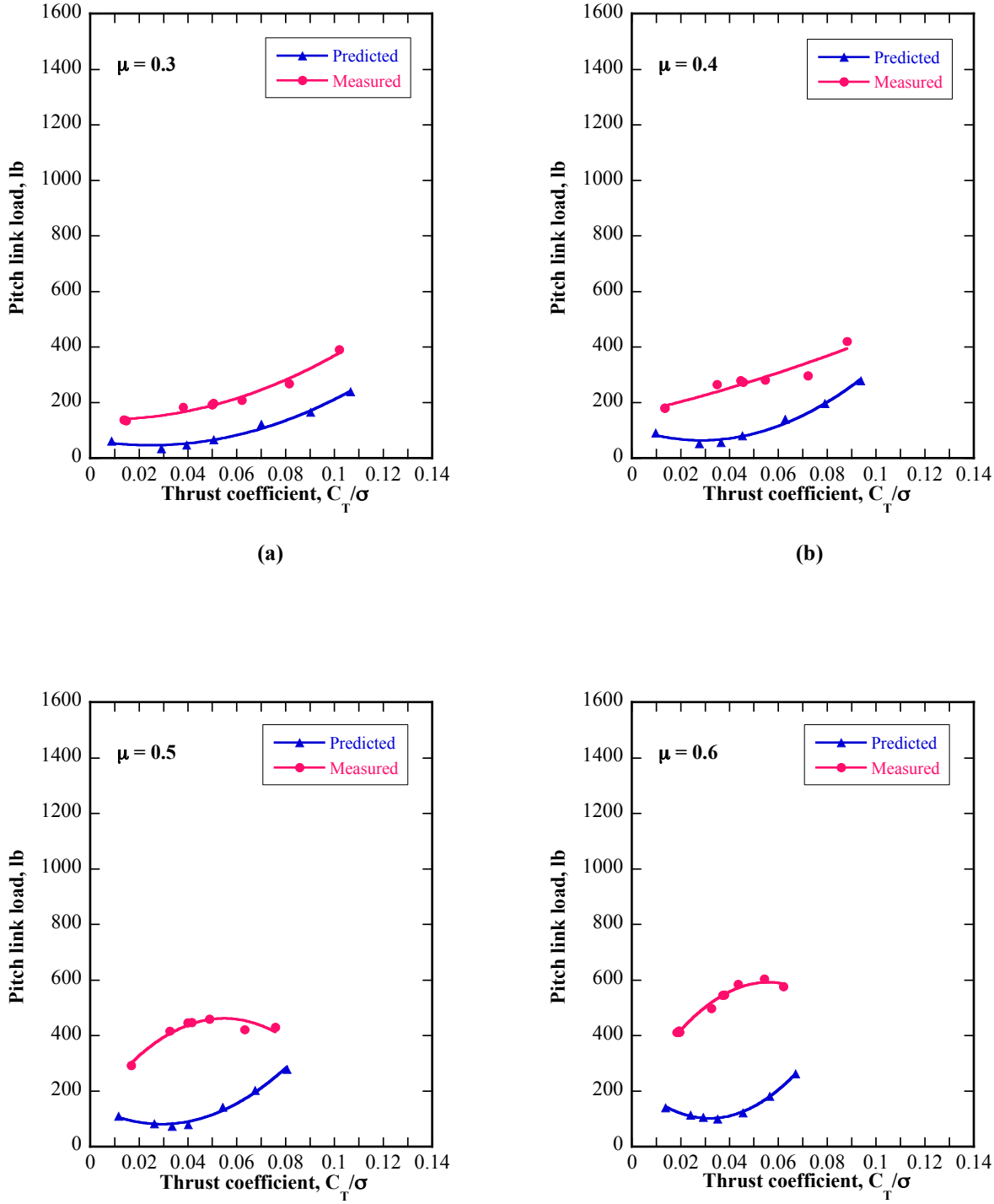

Fig. 13. Half peak-to-peak pitch link load correlation, $\alpha_s = 0^o$, 40%NR.

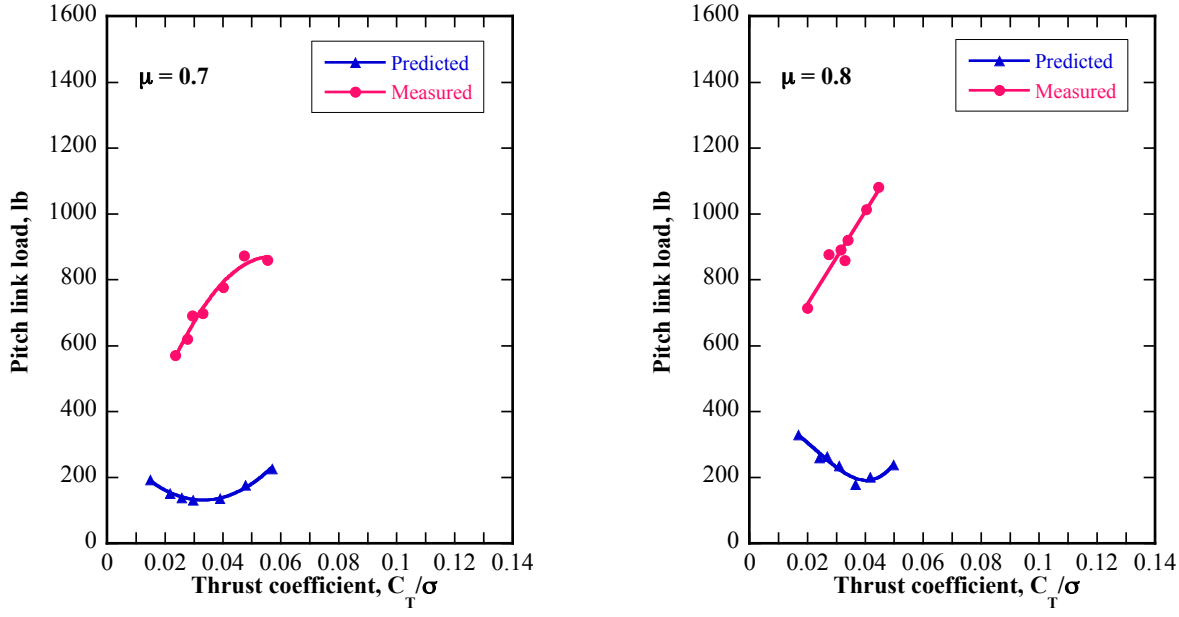

(e)

(f)

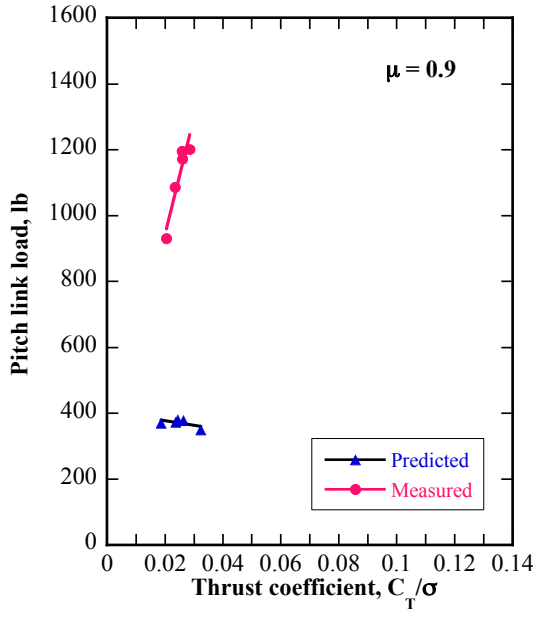

(g)

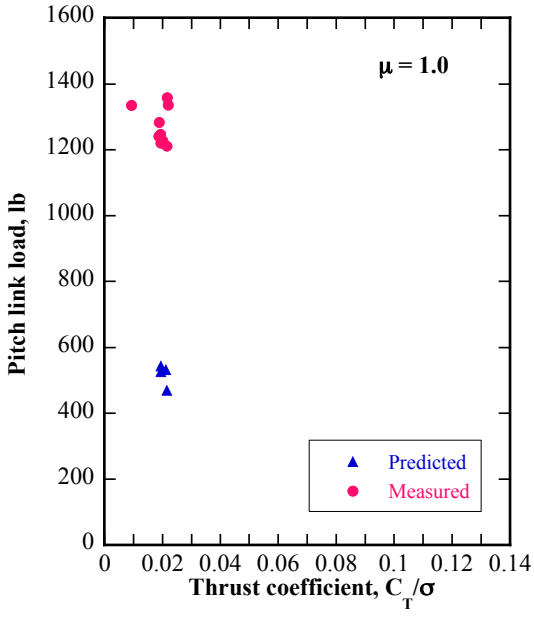

(h)

Fig. 13. cont'd, Half peak-to-peak pitch link load correlation, $\alpha_s = 0^o$, 40%NR.

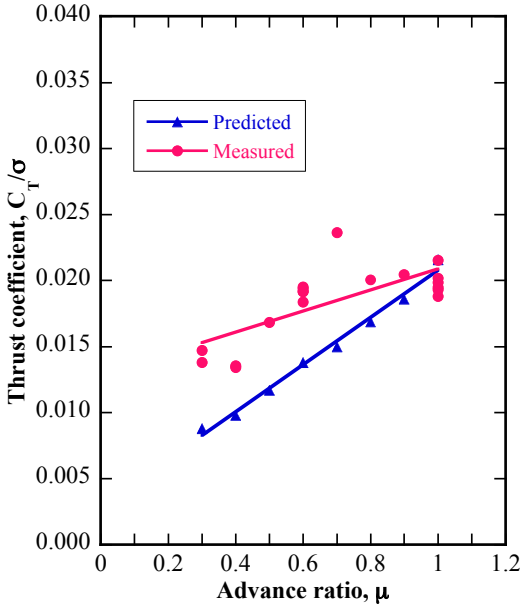

Fig. 14a. UH-60A thrust coefficient, 0^o collective, $\alpha_s = 0^o$, 40%NR.

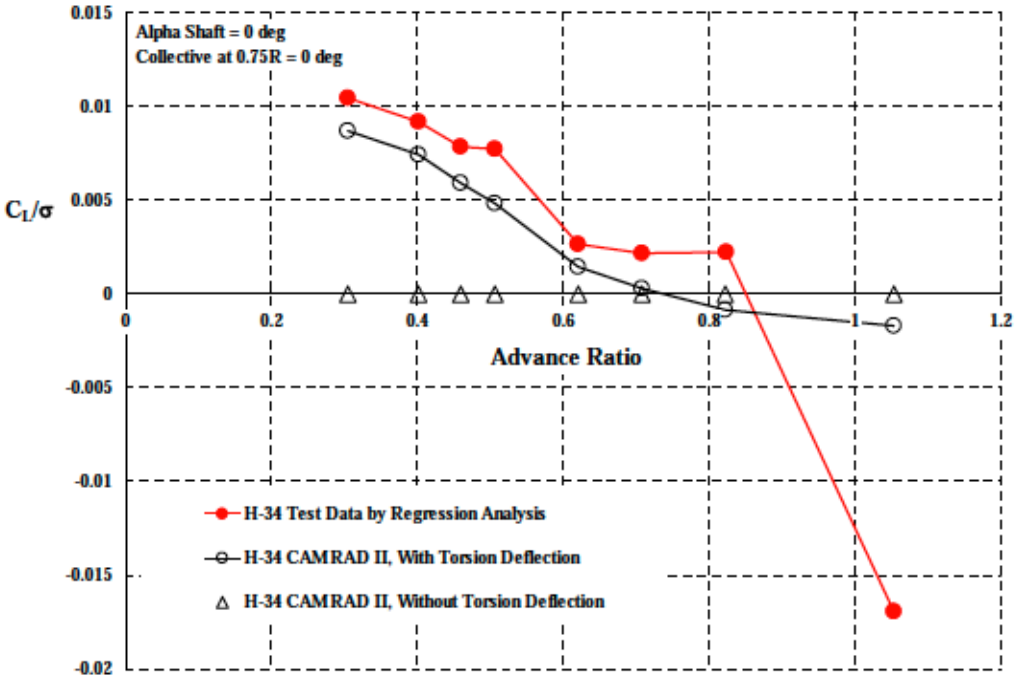

Fig. 14b. H-34 lift coefficient, 0^o collective, $\alpha_s = 0^o$, Fig. 7-6, p. 117, Ref. 2.

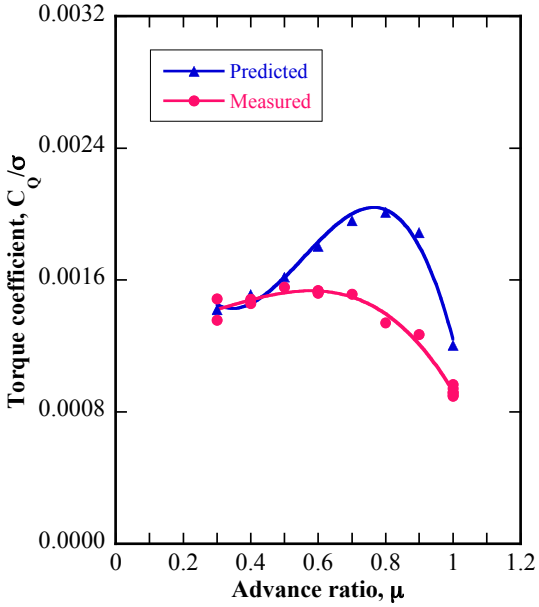

Fig. 15a. UH-60A torque coefficient, 0^o collective, $\alpha_s = 0^o$, 40%NR.

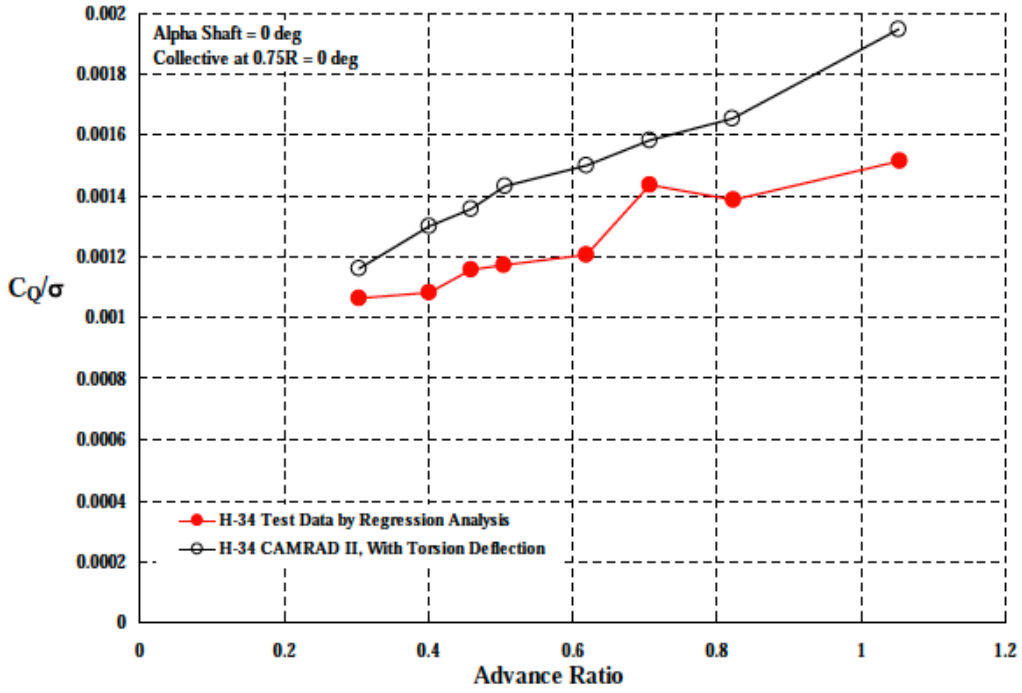

Fig. 15b. H-34 torque coefficient, 0^o collective, $\alpha_s = 0^o$, Fig. 7-11, p. 121, Ref. 2.

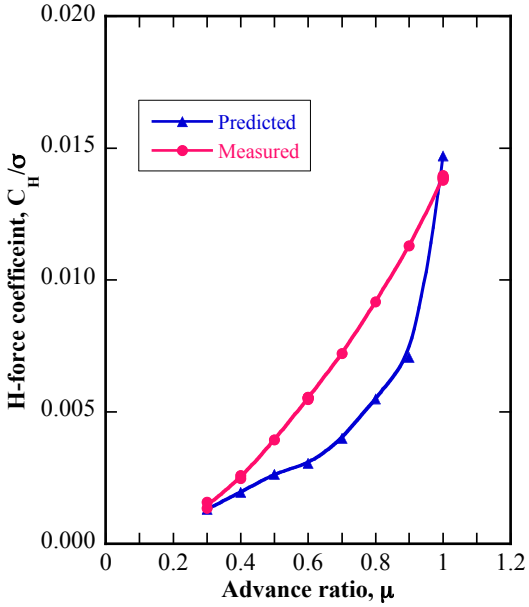

Fig. 16a. UH-60A H-force coefficient, 0° collective, α_s = 0°, 40%NR.

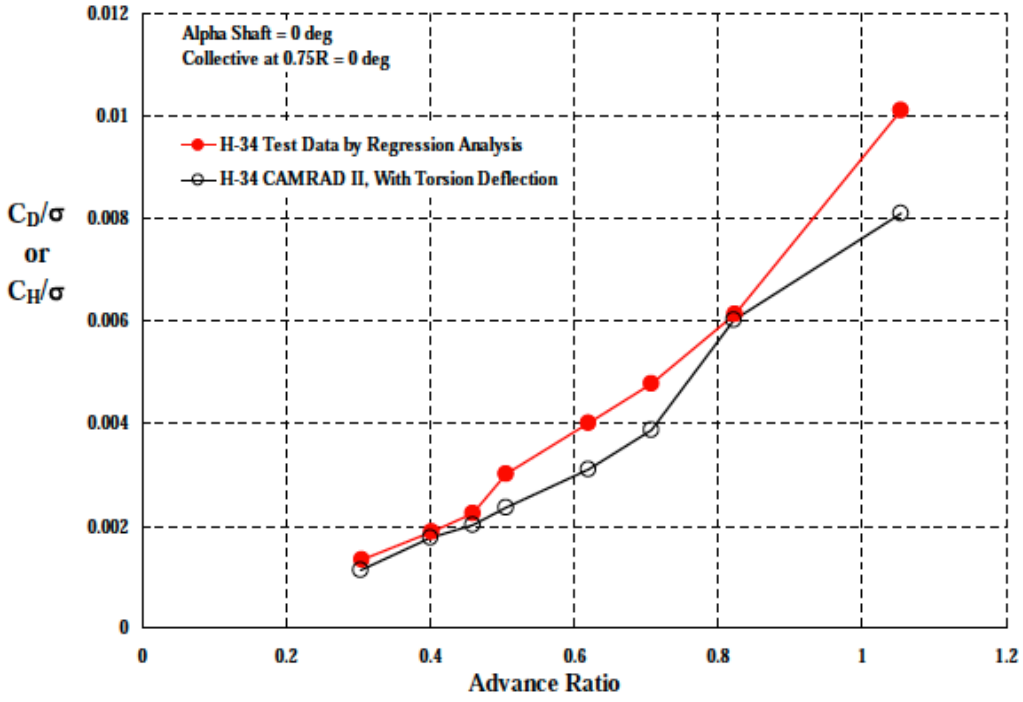

Fig. 16b. H-34 H-force coefficient, 0° collective, α_s = 0° Fig. 7-9, p. 120, Ref. 2.